CRREL
REPORT 84-5

US Army Corps of Engineers
Cold Regions Research & Engineering Laboratory

Morphology and ecology of diatoms in sea ice from the Weddell Sea

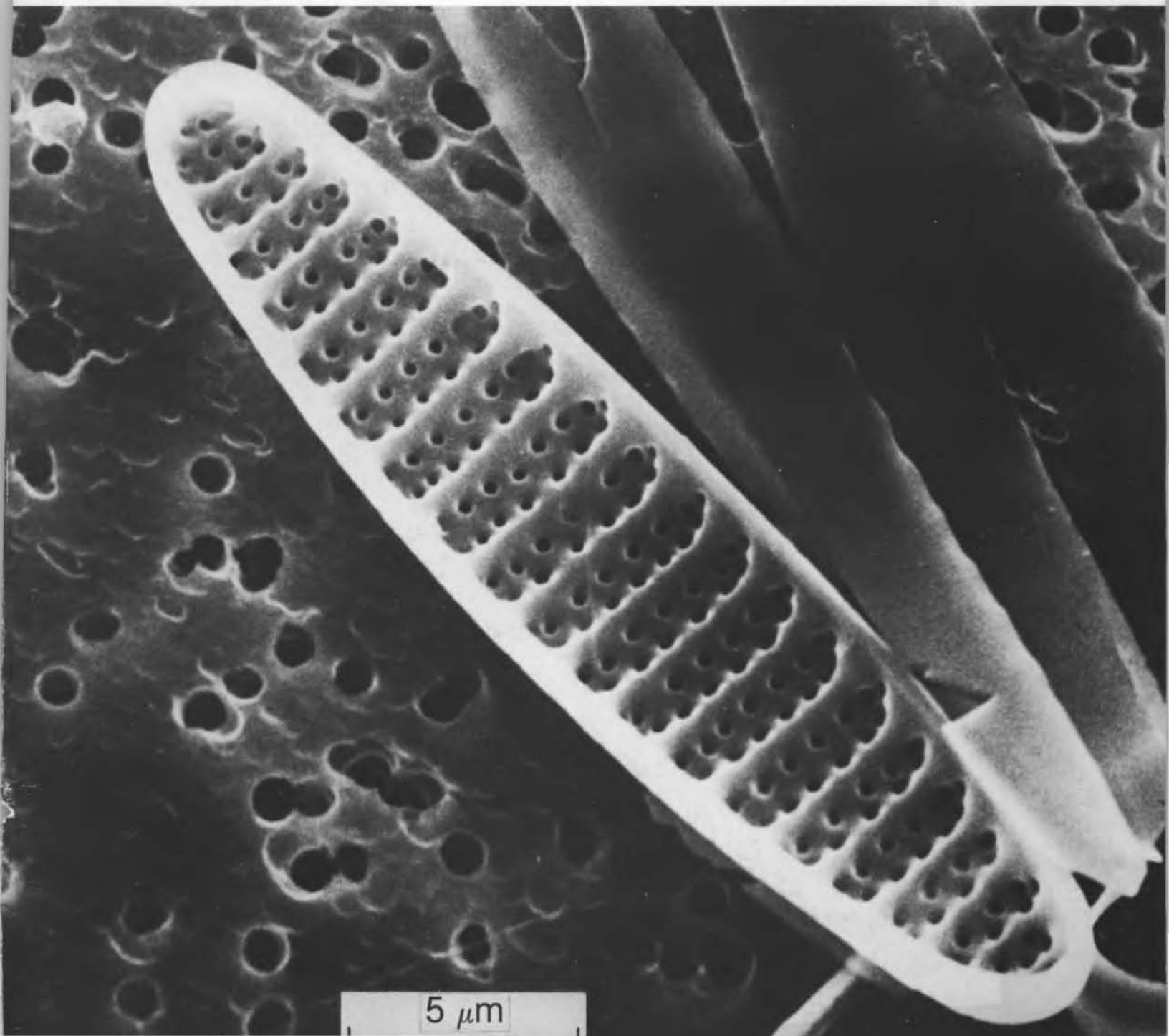

CRREL Report 84-5

February 1984

Morphology and ecology of diatoms in sea ice from the Weddell Sea

D.B. Clarke, S.F. Ackley and M. Kumai

Unclassified

SECURITY CLASSIFICATION OF THIS PAGE *(When Data Entered)*

REPORT DOCUMENTATION PAGE		READ INSTRUCTIONS BEFORE COMPLETING FORM
1. REPORT NUMBER CRREL Report 84-5	2. GOVT ACCESSION NO.	3. RECIPIENT'S CATALOG NUMBER
4. TITLE *(and Subtitle)* MORPHOLOGY AND ECOLOGY OF DIATOMS IN SEA ICE FROM THE WEDDELL SEA		5. TYPE OF REPORT & PERIOD COVERED 6. PERFORMING ORG. REPORT NUMBER
7. AUTHOR(s) D.B. Clarke, S.F. Ackley and M. Kumai		8. CONTRACT OR GRANT NUMBER(s) DPP80-06922-A03
9. PERFORMING ORGANIZATION NAME AND ADDRESS U.S. Army Cold Regions Research and Engineering Laboratory Hanover, New Hampshire 03755		10. PROGRAM ELEMENT, PROJECT, TASK AREA & WORK UNIT NUMBERS
11. CONTROLLING OFFICE NAME AND ADDRESS		12. REPORT DATE February 1984 13. NUMBER OF PAGES 46
14. MONITORING AGENCY NAME & ADDRESS*(if different from Controlling Office)*		15. SECURITY CLASS. *(of this report)* Unclassified 15a. DECLASSIFICATION/DOWNGRADING SCHEDULE

16. DISTRIBUTION STATEMENT *(of this Report)*

Approved for public release; distribution unlimited.

17. DISTRIBUTION STATEMENT *(of the abstract entered in Block 20, if different from Report)*

18. SUPPLEMENTARY NOTES

19. KEY WORDS *(Continue on reverse side if necessary and identify by block number)*

Antarctic region
Diatoms
Morphology
Phytoplankton
Sea ice
Taxonomy

20. ABSTRACT *(Continue on reverse side if necessary and identify by block number)*

Diatom species composition and relative abundances were determined for ice cores obtained from Weddell Sea pack ice during the October-November 1981 Weddell Polynya Expedition (WEPOLEX). Ice thickness and salinity indicate that the ice was less than one year old. The predominant ice type (70%) was frazil, which has the capacity to mechanically incorporate biological material through nucleation and scavenging. Diatoms were found throughout the length of the cores. Species showed down-core fluctuations in abundance that appeared to be correlated with changes in ice type. Pennate forms were more abundant than centrics, the average ratio being 16:1. Diatom frustules with intact organic material were more abundant (5×10^7 cells/liter). Differences in species abundances are attributed initially to incorporation of algal cells from a temporally changing water column and subsequently to diatom reproduction within the ice.

DD FORM 1 JAN 73 1473 EDITION OF 1 NOV 65 IS OBSOLETE

Unclassified

SECURITY CLASSIFICATION OF THIS PAGE *(When Data Entered)*

20. Abstract (cont'd).

Scanning electron micrographs illustrating the morphologic characteristics of the predominant species are included.

PREFACE

This report was written by Diane B. Clarke, Biology Laboratory Technician, and Stephen F. Ackley, Supervisory Physical Scientist, of the Snow and Ice Branch, and by Dr. Motoi Kumai, Research Physicist, of the Earth Sciences Branch, Research Division, U.S. Army Cold Regions Research and Engineering Laboratory, Hanover, New Hampshire. The study was supported by National Science Foundation Agreement DPP80-06922-A03 dated June 1983, *Air-Sea Interaction and Sea Ice Studies of the Joint US/USSR Weddell Polynya Expedition.*

The authors would like to thank three individuals at Texas A&M University for their help and support: G.A. Fryxell for use of her inverted light microscope and ancillary laboratory equipment as well as her wonderful collection of reference materials and her helpful discussions; K.R. Buck, for his help and expertise in Choanoflagellate and diatom identifications; and L.K. Medlin, for her assistance with Naviculoid diatom identifications. L.V. Parker and J.A. Richter-Menge critically reviewed this manuscript.

CONTENTS

ILLUSTRATIONS

Figure

TABLES

Table

MORPHOLOGY AND ECOLOGY OF DIATOMS IN SEA ICE FROM THE WEDDELL SEA

D.B. Clarke, S.F. Ackley and M. Kumai

INTRODUCTION

Diatoms are major primary producers of microbial biomass in the Antarctic. They are found both in the water column and in sea ice. Primary production of diatoms in the water column has been used in the past to determine the productivity of the Southern Ocean.

During the winter, sea ice covers 20 $\times$ 10^6 km^2 of the Southern Ocean surface, but in the summer melts back to cover 3 $\times$ 10^6 km^2. Two processes enhance the effect of sea ice on primary production. From fall to spring, sea ice reduces light penetration, thereby diminishing production in the water. As light returns in the spring, diatoms in the ice begin to reproduce (Buynitsky 1977, Hoshiai 1977, Meguro et al. 1967). In the late spring, as the ice melts, the diatoms contained in the sea ice are released into the water column. Depending on the extent of reproduction within the ice, the potential contribution of diatoms in sea ice to overall productivity could be significant.

Measurements of chlorophyll *a* concentrations indicate the amount of viable plant material present. Peak chlorophyll *a* concentrations ranging from 3.8 to 2100 mg/m^3 have been reported for different ice types and are considerably higher than in adjacent surface waters (Ackley et al. 1979, Bunt 1963, Burkholder and Mandelli 1965, Clarke and Ackley, in press, Garrison and Buck, in prep., Hoshiai 1977, Meguro 1962, Sullivan and Palmisano 1981). One question to consider is whether these concentrations are due to mechanical incorporation alone or are a result of diatom growth in a protected environment.

Three different ice types (frazil, congelation, and snow ice) have been found in the drifting pack of the Weddell Sea (Clarke and Ackley, in press). Weeks and Ackley (1982) have described in detail the formation processes for both frazil and congelation ice. Briefly, frazil ice is associated with dynamic, turbulent conditions in the water column where small ($\sim$ 1 mm) ice crystals form, usually at high growth rates ($>$1 cm/hr). These crystals are advected downstream by wind-induced circulation in the water column and pile up into substantial thicknesses of ice in a short time period. Gow et al. (1982) reported up to 50% frazil ice during their 1980 cruise, while Clarke and Ackley (1982) and Ackley et al. (1982) found a predominance of frazil (70%) during their 1981 cruise. In direct contrast to frazil ice, congelation ice forms as large columnar grained crystals ($\sim$ 1 cm) resulting from the slow removal of heat from the water under an existing ice sheet. After a few centimeters of ice have formed, the low thermal conductivity of the ice limits the heat transfer and prevents growth rates greater than 1 mm/hr, and the rate continues to decrease as the ice thickens. Congelation ice therefore forms more slowly and over periods on the order of several weeks to achieve the thicknesses reported by Clarke and Ackley (1982). The third ice type—snow ice—is associated with the ridge-building process in the

Weddell region. Ice floes in the Weddell Sea may be covered by up to 30 cm of snow (Clarke and Ackley, in press). As ice floes collide and deform, they form ridges, the ice sheet is depressed below sea level by the weight of the ice piled up in the ridge, and the snow at the base of these ridges often becomes infiltrated with sea water. Subsequent freezing creates snow ice.

From prior observations it appears that frazil ice initially concentrates biological material, whereas congelation ice tends to reject it. Ackley (1982) and Garrison et al. (in press) have suggested two physical mechanisms to account for the high concentrations of algae in young, thin ice samples: scavenging and nucleation. Reproduction alone cannot be responsible for high concentrations in this ice since doubling times are insufficient relative to the age of the ice. A conservative estimate of the age of the ice is 24 hours, the ice growth rate being 1 cm hr^{-1} (Weeks and Ackley 1982). The chlorophyll concentration is up to 50 times higher in the ice than in the surface water. Therefore, using a doubling time of 0.75 doublings/day^{-1}, a minimum of 8 days would be required. Ackley (1982) and Garrison et al. (in press) suggest that concentration by ice nucleation occurs when frazil ice crystals nucleate on suspended algal cells. In addition, ice scavenging occurs as a frazil ice crystal travels through the water column to the surface and collides with particles along the way. Unlike nucleation, through scavenging, each frazil ice crystal may collect several particles rather than only one.

Contrary to expectation, however, the highest chlorophyll values reported are from congelation ice near McMurdo Sound and Syowa Station (248–2100 mg/m^3) rather than from frazil ice (Bunt 1963, Hoshiai 1977, Sullivan and Palmisano 1981). Intermediate values are found in the snow ice from Syowa Station and off the Palmer Peninsula (407–670 mg/m^3) (Burkholder and Mandelli 1965, Meguro 1962), and the lowest values are found in the predominantly frazil ice of the Weddell Sea (3.8–29.7 mg/m^3) (Ackley et al. 1979, Clarke and Ackley, in press, Garrison and Buck, in press). Thus it would appear that several processes (scavenging, nucleation, and growth) are responsible for algal concentrations, depending on the ice type. To determine to what extent the physical environment of the ice affects the biological community, we compared the species composition and abundance between cores with only one ice type and those with alternating ice types.

In addition to ice algae's potential contribution to total productivity, it has been hypothesized that they may be a "seed population" that is responsible for the spring bloom in the water column. Diatoms that are still viable after overwintering in the ice may be the nucleus of the spring growth after meltout. To confirm this it is necessary to determine species composition in the ice, rather than just chlorophyll concentrations, and to identify those cells with intact organic material. To this end we have examined settled samples under an inverted light microscope to determine the ratio of empty to full cells. We have also delineated the species composition in our Weddell Sea pack ice samples with illustrative scanning electron microscope (SEM) micrographs of the morphologic characteristics of each species for future comparisons with water column assemblages.

The SEM provides the high resolution necessary to resolve internal and external features and thus allows positive species identification. Some of the morphologic features that are readily apparent under SEM, but not always under the light microscope, are the central, labiate, and marginal processes of the *Thalassiosira* and the labiate and strutted processes of the *Porosira* (see Appendix B for terminology). Other features, indistinguishable without SEM, are the puncta forming the the fine striae on some of the *Nitzschias* or the puncta on the girdle bands of several centric species. In addition, some of the *Nitzschia* specimens in our samples are quite small (2–5 μm) and would not be identifiable without the SEM.

MATERIALS AND METHODS

During a cooperative scientific expedition (WEPOLEX) between the United States and the U.S.S.R., the NES *Mikhail Somov* maneuvered within the pack ice of the Weddell Sea from 22 October to 13 November 1981 (Fig. 1) (Gordon and Sarukhanyan 1982). Two types of ice samples were obtained: ice cores and ice chunks. The cores were drilled using a USACRREL 7.6-cm ice-coring auger, while chunks weighing a few kilograms and composed primarily of snow ice were retrieved either from the open water cleared by the ship or from newly formed ice ridges. Different techniques were employed to prepare samples for examination with the SEM and the optical and inverted light microscopes.

For optical light microscope analysis, the samples were melted and filtered through a 0.4-μm Millipore or Nucleopore filter. The diatoms were then washed off the filter and decanted into centrifuge tubes. Additional distilled water was added

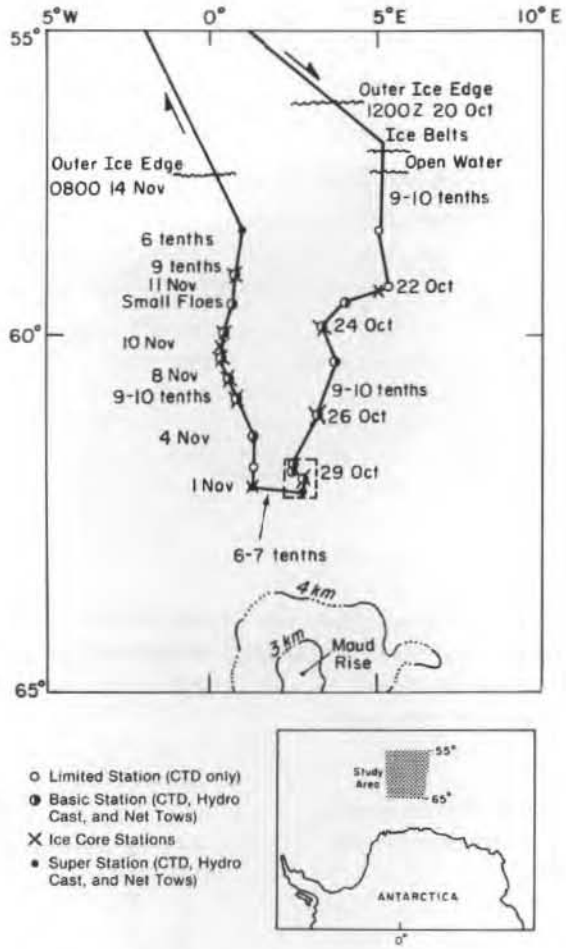

Figure 1. Cruise track of the NES Mikhail Somov *during the U.S.-U.S.S.R. Weddell Polynya Expedition, October–November 1981, and the relationship of the study area to Antarctica. Total ice cover in the area is given in tenths.*

to each sample to bring the total volume to 90 ml. The samples were then centrifuged for 5 minutes at 1500 rpm, the supernatant liquid was siphoned off, and more distilled water was added. This rinsing procedure was repeated three times to remove salt crystals. After the last rinse, 0.1 ml of the residue was pipetted onto a 24 × 50 mm coverslip and heated until dry. The coverslip was then affixed to a glass slide using Aroclor 5442 (refractive index 1.6) and was subsequently observed under a Leitz optical light microscope with a 100X oil immersion lens (total magnification 1000X).

For the SEM study, the samples were melted and then cleaned of organic material to obtain optimum clarity. Fifty milliliters each of hydrogen peroxide (30%) and hydrochloric acid (30%) were added to a melted sample, which was gently boiled for 20 minutes. Distilled water was added to bring the volume to 1 liter, and the sample was transferred to centrifuge tubes. The rinsing procedure cited above was used to remove inorganic residues and salt crystals. Subsequently, 3 to 20 ml of sample was filtered through a 0.4-μm Nucleopore filter to obtain a suitable concentration of diatoms. The filter was affixed with double-stick tape to a sample mount and coated with palladium-gold (40:60) vapor to a thickness of about 100 Å in a vacuum chamber. An accelerating voltage of 20 kV was used to examine the sample on a Hitachi S-500 SEM.

Samples for the inverted light microscope were melted and several milliliters of 4% buffered formaldehyde were added. Samples were agitated and 10 ml was poured into a counting chamber.

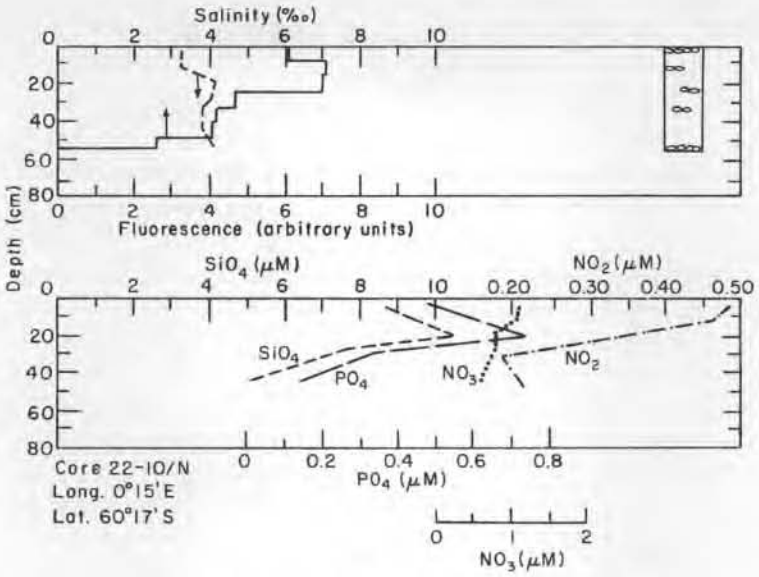

Figure 2. Core profile of 22-10/N showing salinity, fluorescence, nutrients (silicic acid, phosphate, nitrate, nitrite), and structure vs depth. In the structural cartoon, circles indicate frazil ice structure.

The aliquot was allowed to settle for 24 hours prior to examination under a Zeiss microscope (total magnification 500–800X).

RESULTS

Two ice cores and an ice chunk were obtained on 10 November 1981, at 60° 17'S, 0° 15.3'E. The ice chunk (10–N/K) was composed of snow ice (sea-water-infiltrated snow); ice core 22–10/N (54 cm long) was all frazil ice; and ice core 23–10/N (59 cm long) had 16 cm of congelation ice at the bottom overlain by 43 cm of frazil ice. Structural and salinity profiles for these two cores are shown in Figures 2 and 3.

Samples of the ice chunk were examined under the SEM and the optical light microscope, samples of core 22–10/N were examined under the SEM and the optical and inverted light microscopes, and samples of core 23–10/N were only observed under the inverted light microscope. When comparing species differences, therefore, one must take into account the different preparation techniques involved as well as the optical qualities of the microscopes. These differences as they pertain to different techniques are discussed in Appendix B.

Figures 4a and 4b are schematic representations of pennate and centric diatom frustules illustrating their various components. Some of the more common morphologic characteristics used to identify species are the valve outline and dimensions, the pattern of areolation, the presence or absence of a raphe or pseudoraphe, the type and arrangement of processes, and the number and arrangement of intercostal poroids. (Appendix B defines the taxonomic features.) Whole frustules (Fig. 5) as well as separated valves (Fig. 6) and girdle bands (Fig. 7) were observed under the SEM, but relatively few fragments were

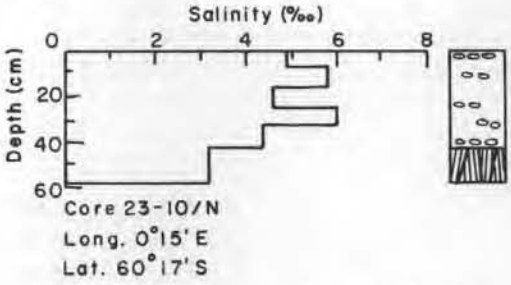

Figure 3. Core profile of 23–10/N showing salinity, fluorescence, nutrients (silicic acid, phosphate, nitrate, nitrite), and structure vs depth. In the structural cartoon, circles indicate frazil ice structure and vertical lines show congelation or columnar ice structure.

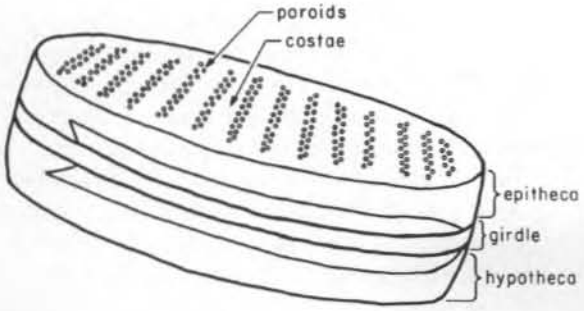

a) Pennate diatom showing the two valve halves, girdle bands, costae, and poroids.

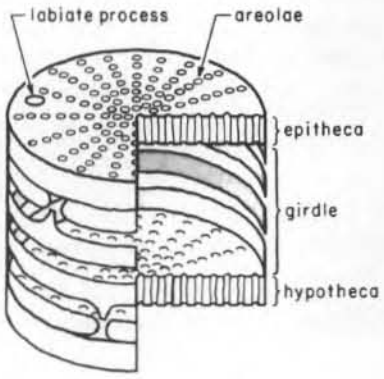

b) Centric diatom showing the two valve halves, girdle bands, areolae, and labiate process.

Figure 4. Schematic representations of diatoms.

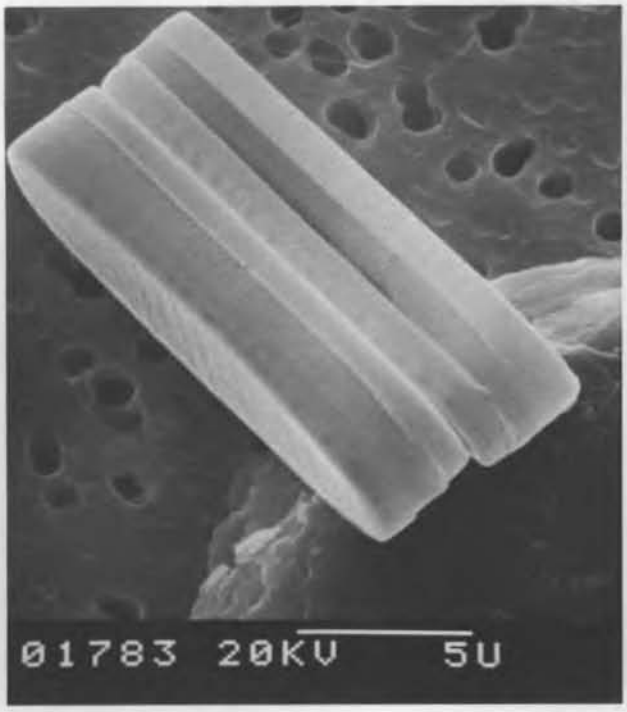

Figure 5. Nitzschia *sp. 2 complete frustules (oblique view). Costae and poroids on valve face are visible, as are the girdle bands. White bar at bottom = 5 μm.*

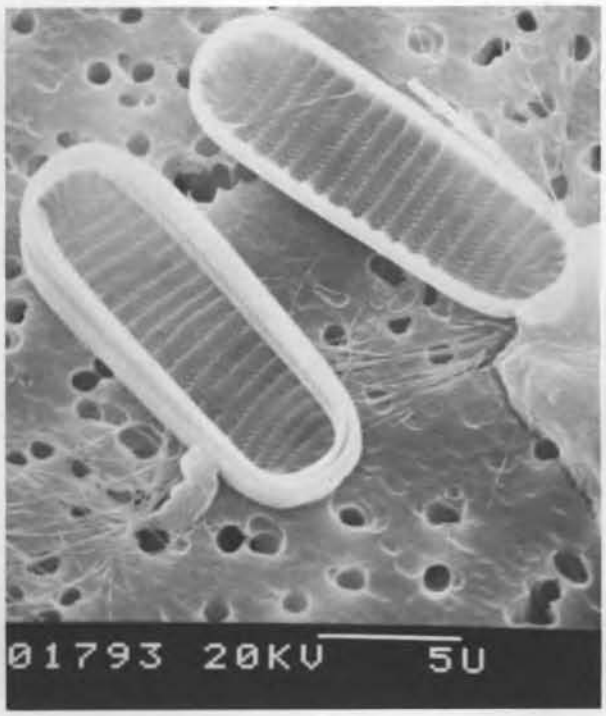

Figure 6. Nitzschia curta. *Two valves of a frustule (interior) with girdle bands still attached to both valves. Costae and double rows of poroids are evident. White bar at bottom = 5 μm.*

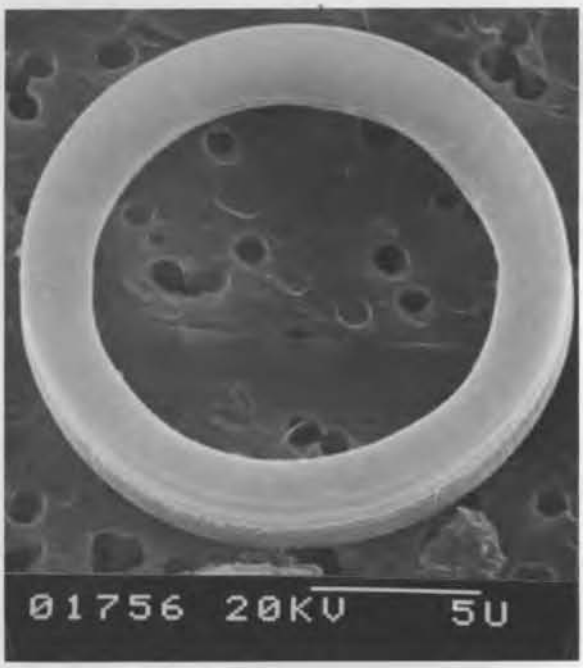

found. Undoubtedly the separation of most of the frustules was a result of the acid-cleaning technique we employed. For the most part, the valves were in good condition. The setae of *Chaetoceros* were the most susceptible to breakage.

In the three samples taken on 10 November 12 genera and 33 species were identified. Of these, eight species were not identified at the species level but were given numeric designations. Fifteen of the species were observed in only one of the three samples. Of these, only three (*Chaetoceros neglectum* Karsten, *Nitzschia lecointei* Van Heurck, and *Thalassiosira gravida* Cleve) were seen more than once in a sample, but still not in significant quantities. Table 1 lists all of the species identified from

Figure 7. Girdle bands of a centric diatom (oblique view). White bar at bottom = 5 μm.

Table 1. Diatoms identified under optical, inverted, and scanning electron microscopes.

Composite species list	*Present in 10/N-K*	*22-10/N*	*23-10/N*
Actinocyclus actinochilus (Ehrenberg) Simonsen	+	+	
Asteromphalus hyalinus Karsten	+		
Chaetoceros dichaeta Ehrenberg	+	+	+
Chaetoceros gracilis Schutt	+	+	+
Chaetoceros neglectum Karsten	+		
Chaetoceros sp. 7	+	+	
Dactyliosolen antarcticus Castracane	+	+	+
Navicula sp. 1	+	+	+
Navicula sp. 2	+		
Nitzschia angulata Hasle	+	+	+
Nitzschia closterium (Ehrenberg) W. Smith	+	+	+
Nitzschia curta (Van Heurck) Hasle	+	+	+
Nitzschia cylindrus (Grunow) Hasle	+	+	+
Nitzschia kerguelensis (O'Meara) Hasle	+	+	+
Nitzschia lecointei Van Heurck			+
Nitzschia prolongatoides Hasle			+
Nitzschia ritscheri (Hustedt) Hasle	+	+	
Nitzschia subcurvata Hasle	+	+	+
Nitzschia turgiduloides Hasle	+	+	+
Nitzschia sp. 1	+		
Nitzschia sp. 2		+	
Porosira pseudodenticulata (Hustedt) Jouse	+	+	
Rhizosolenia alata Brightwell	+		
Synedra sp. 1		+	
Thalassiosira ambigua Kozlova	+		
Thalassiosira frenguelli Kozlova	+		
Thalassiosira gracilis var. *gracilis* (Karsten) Hustedt	+	+	
Thalassiosira gravida Cleve	+		
Thalassiosira lentiginosa (Janisch) Fryxell	+	+	
Thalassiosira sp. 1		+	
Thalassiosira sp. 2	+		
Thalassiothrix antarctica Shimper			+
Tropidoneis glacialis Heiden	+	+	+

Table 2. All species identified under the inverted light microscope in ice cores 22-10/N and 23-10/N and the number of full and empty cells/liter of each.

Species	22-10/N		23-10/N	
	Full	*Empty*	*Full*	*Empty*
Chaetoceros dichaeta	1.2×10^4	—	6.2×10^3	5.3×10^3
Chaetoceros gracilis	4.0×10^3	—	3.6×10^4	8.2×10^3
Dactyliosolen antarcticus	—	—	4.7×10^4	3.6×10^4
Navicula sp. 1	1.2×10^4	—	4.5×10^4	—
Nitzschia angulata	—	—	3.0×10^3	—
Nitzschia closterium	1.76×10^3	3.0×10^4	1.5×10^4	1.2×10^3
Nitzschia curta	—	—	2.2×10^4	2.5×10^4
Nitzschia cylindrus	1.2×10^4	—	1.7×10^4	2.3×10^3
Nitzschia kerguelensis	—	—	3.5×10^4	1.3×10^4
Nitzschia lecointei	—	—	1.3×10^4	—
Nitzschia prolongatoides	—	—	1.7×10^4	2.0×10^3
Nitzschia subcurvata	2.0×10^3	—	2.6×10^3	2.5×10^4
Nitzschia turgiduloides	—	4.0×10^3	2.0×10^3	2.2×10^4
Synedra sp. 1	2.6×10^4	—	—	—
Thalassiothrix antarctica	—	—	—	2.3×10^3
Tropidoneis glacialis	9.6×10^4	1.0×10^4	2.0×10^6	2.6×10^3
Nitzschia (Fragilariopsis group)	—	—	3.8×10^4	1.2×10^3
Totals	3.4×10^5	4.4×10^4	9.0×10^6	1.5×10^6
Archaeomonads	1.4×10^4	2.0×10^3	1.9×10^4	—
Choanoflagellida	4.0×10^3	—	1.1×10^3	—
Dinophyceae	2.0×10^3	—	3.9×10^3	—
Prymnesiophyceae (*Phaeocystis* cf. *pouchetti*)	2.2×10^6	—	3.3×10^3	—

these samples. They are predominantly composed of pennate forms, with *Tropidoneis glacialis* Heiden, *Nitzschia closterium* (Ehrenberg) W. Smith, *Nitzschia prolongatoides* Hasle, and *Nitzschia cylindrus* (Grunow) Hasle being the major constituents. Brief descriptions of each species, with SEM micrographs to illustrate their morphologic characteristics, are in Appendix C.

After all of the species were identified under SEM, observations were made using optical and inverted light microscopes to obtain relative species abundances and numbers of cells per liter. Although 27 species were identified in the ice chunk, the diatom assemblage was nearly monospecific, with *T. glacialis* accounting for 85–94% of the total. *Nitzschia curta* (Van Heurck) Hasle, *Chaetoceros dichaeta* Ehrenberg, *N. closterium*, and *N. cylindrus* each accounted for 1 to 3%; the remaining species were less than 1% of the total. In both ice cores several species were codominant. In 22-10/N, 21 species were identified. The dominant species were *N. closterium* and *T. glacialis* with *Synedra* sp. 1, *Nitzschia kerguelensis* (O'Meara) Hasle, *N. cylindrus, Ch. dichaeta,* and *Navicula* sp. 1 comprising 4 to 8% each. In 23-10/N, the dominant species were *T. glacialis, N. cylindrus, N. prolongatoides, N. closterium,* and *Ch. dichaeta.* In addition, *Nitzschia subcurvata* Hasle and *Nitzschia turgiduloides* Hasle accounted for 2 to 3% each.

One of the advantages of using the inverted light microscope is that it allows differentiation between full and empty diatom frustules, that is, whether the chloroplasts and other organic material are still intact within the cell. We counted the number of cells per liter that were empty or full in both the ice cores. Due to sampling limitations, 22–10/N was counted as one composite sample but we were able to examine 23–10/N at nominal 10-cm intervals. A composite species list with the total number of cells/liter for each species in the two cores is shown in Table 2. There is a significant difference in the number of species present in each of the two cores as well as a difference in the full/empty cells. Almost twice as many species are present in 23–10/N. There are 10 times more full cells/liter and 20 times more empty cells/liter in 23–10/N. Figure 8 shows the number of cells/liter down the length of 23–10/N. It is evident that the highest concentration of full cells/liter occurs near but not at the bottom of the core. There were 10 times more full cells/liter in the bottom 16 cm than at the surface. The variations in abundance of the dominant species in this

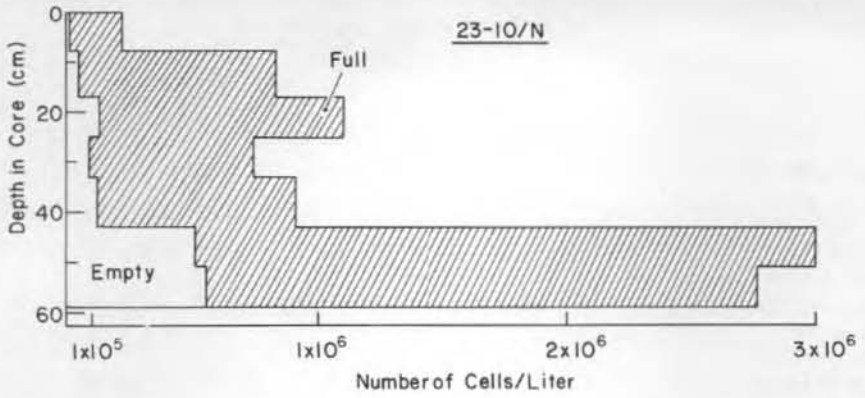

Figure 8. Core profile of 23-10/N showing the total number of empty and full diatom cells/liter vs depth.

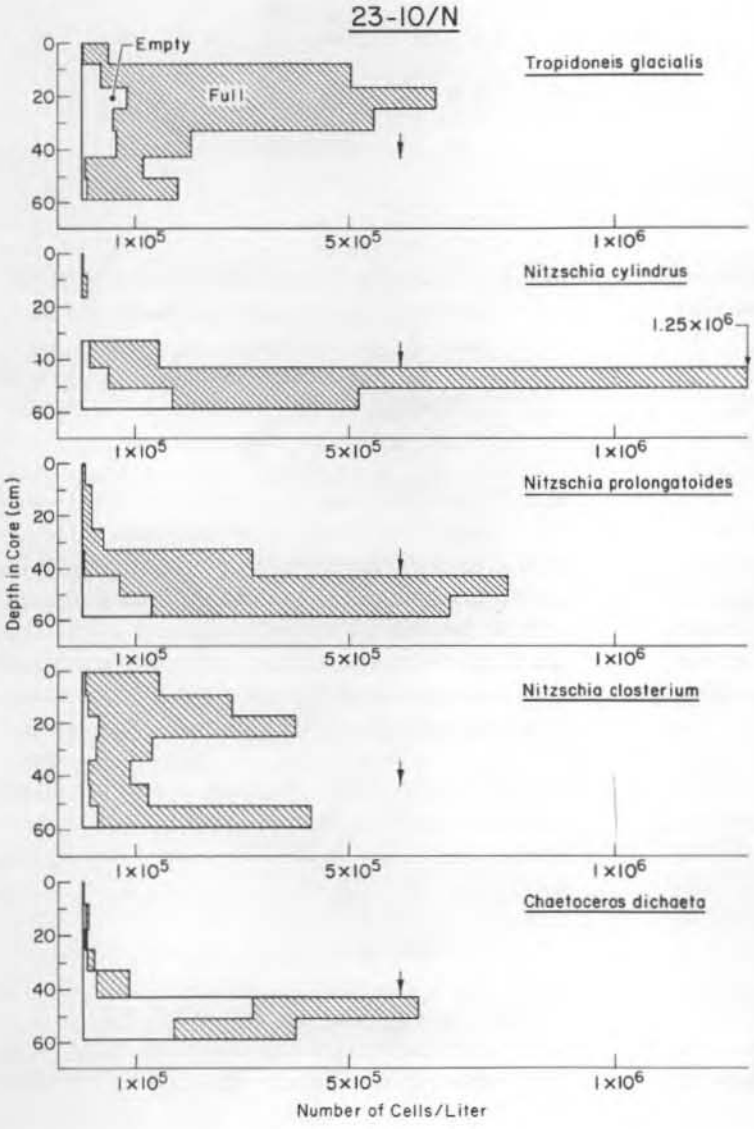

Figure 9. Core profile of 23-10/N showing the number of empty and full cells/liter for each of the abundant species (Tropidoneis glacialis, Nitzschia cylindrus, N. prolongatoides, N. closterium, *and* Chaetoceros dichaeta) *vs depth. The arrow at 43 cm indicates the transition from frazil to congelation ice.*

Table 3. The number of empty and full cells/liter of the abundant species and the total count in each core at the specified depth interval.

Core	Depth (cm)	Empty/liter	Full/liter	Abundant species	Total Empty	Total Full	Ice type
3-24/0	55-63	$(2.4\times10^{6}$	1.8×10^{7}	*N. prolongatoides*	(3.1×10^{6})	2.0×10^{7}*	frazil
4-24/0	33-49	(2.2×10^{6})	1.0×10^{7}	*N. prolongatoides*	(4.2×10^{6})	1.2×10^{7}*	frazil
9-1/N	17-36	(2.8×10^{4})	7.3×10^{5}	*N. subcurvata*			
		(1.4×10^{4})	4.5×10^{5}	*N. turgiduloides*	(1.4×10^{6})	1.8×10^{6}	frazil
		(1.0×10^{6})	2.7×10^{5}	*N. prolongatoides*			
14-4/N	44-58	(2.0×10^{7})	4.9×10^{5}	*N. prolongatoides*			
		(2.0×10^{7})	3.9×10^{5}	*N. cylindrus*	(3.4×10^{6})	1.4×10^{9}	congelation
		(5.4×10^{7})	1.4×10^{5}	*Ch. dichaeta*			
17-8/N	23-53	(9.7×10^{4})	7.1×10^{5}	*N. prolongatoides*			
		(1.0×10^{5})	4.0×10^{5}	*N. closterium*	(4.1×10^{5})	1.3×10^{6}*	congelation
22-10/N	0-54	(3.0×10^{4})	1.8×10^{5}	*N. closterium*			
		(1.0×10^{4})	9.6×10^{4}	*T. glacialis*	(4.4×10^{4})	3.4×10^{5}*	frazil
23-10/N	0-59	(2.6×10^{5})	2.0×10^{6}	*T. glacialis*			
		(2.3×10^{5})	1.7×10^{6}	*N. cylindrus*	(1.5×10^{6})	9.0×10^{6}	frazil/congelation
		(2.0×10^{5})	1.7×10^{6}	*N. prolongatoides*			
		(1.2×10^{5})	1.5×10^{6}	*N. closterium*			
24-11/N	32-69	(1.0×10^{5})	8.7×10^{4}	*N. cylindrus*			
		(5.0×10^{4})	3.5×10^{5}	*Navicula* sp. 1	(7.6×10^{5})	2.4×10^{6}*	frazil/congelation
		(7.2×10^{4})	2.4×10^{5}	*N. closterium*			
26-13/N	0-54	(1.5×10^{5})	4.0×10^{5}	*N. closterium*			
		(6.9×10^{5})	1.0×10^{6}	*Navicula* sp. 1	(4.0×10^{5})	8.2×10^{5}	frazil/congelation

* 10 times greater full than empty.

core are shown in Figure 9. It is obvious that three of the species (*N. cylindrus, N. prolongatoides,* and *Ch. dichaeta*) are most abundant near the bottom, while *T. glacialis* is highest just below the surface and *N. closterium* has a bimodal curve with two equal peaks, one just below the surface and the second at the bottom.

Seven additional cores were examined under the inverted light microscope, three composed solely of frazil ice, two of congelation ice, and two a combination of these two ice types (Table 3). None of these cores was examined at discrete 10-cm depth intervals, but rather as a composite sample ranging from 8 to 54 cm (the whole core); the average sample interval was 20 cm. Among these samples, two had monospecific assemblages (>85%) of *N. prolongatoides* and the remainder had assemblages comprising several co-dominant species (Table 3). The diatoms that comprised the remainder of a sample were the same as those in cores 22- and 23-10/N.

A comparison of the number of full to empty diatom cells/liter in all the ice cores examined shows that in all but one instance there were more full than empty cells, and in half of the cores there were 10 times as many full cells as empty cells (Table 3). Looking at the individual plots of cells/liter for the most abundant species in 23-10/N (Fig. 9), it is obvious that at each major peak (regardless of where in the core it occurs) the increase in full cells/liter is considerable, while for the empty cells/liter it is not. Chlorophyll *a* values in the ice cores at the same depths for which we have diatom counts ranged from 0.09 to 0.672 mg/m^3. Phaeophytin values over these same intervals ranged from 0.04 to 0.19 mg/m^3. Although we would have liked to compare the chlorophyll and phaeophytin values with the full and empty cells/liter, the number of samples for which we have both data sets is too small to be significant. The highest chlorophyll *a* concentrations were found in the ice chunks, ranging from 0.14 to 43.2 mg/m^3. The phaeophytin in these chunks ranged from 0.03 to 15.9 mg/m^3. Chlorophyll values in all of the cores and ice chunks were higher than in the adjacent surface waters (0.07–0.13 mg/m^3).

In addition to the diatoms (Bacillariophyceae), which were the most abundant group, representatives of several other groups—Choanoflagellida, Chrysophyceae, Dinophyceae, Gymnodiniaceae, Prymnesiophyceae, siliceous cysts, and archaeomonads—were also found.

Two archaeomonad species, *Archaeomonas areolata* Deflandre and *Litheusphaerella spectabilis* Deflandre (Fig. 10), were observed in several of our samples (see, for example, Table 2) in relatively low concentrations ($\geq10^4$). Until recently, archaeomonads had not been reported

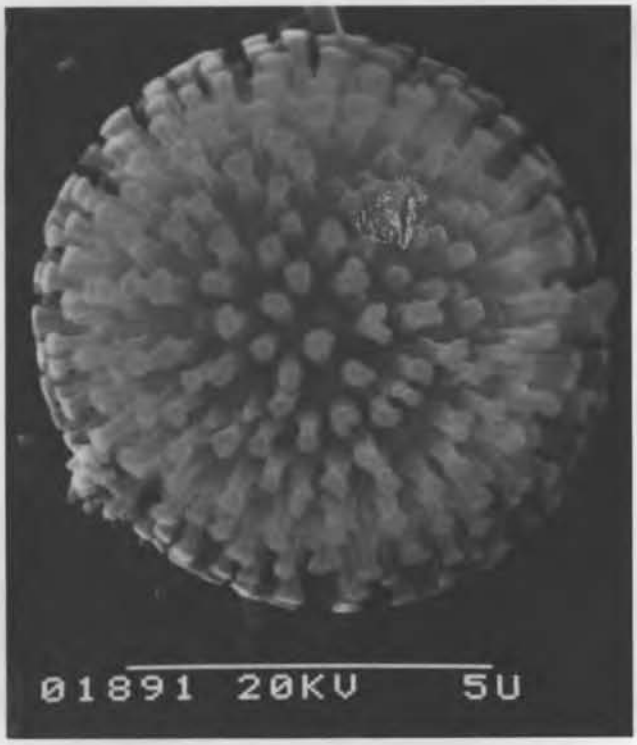

Figure 10. Archaeomonad: Litheusphaerella spectabilis. *White bar at bottom = 5 μm.*

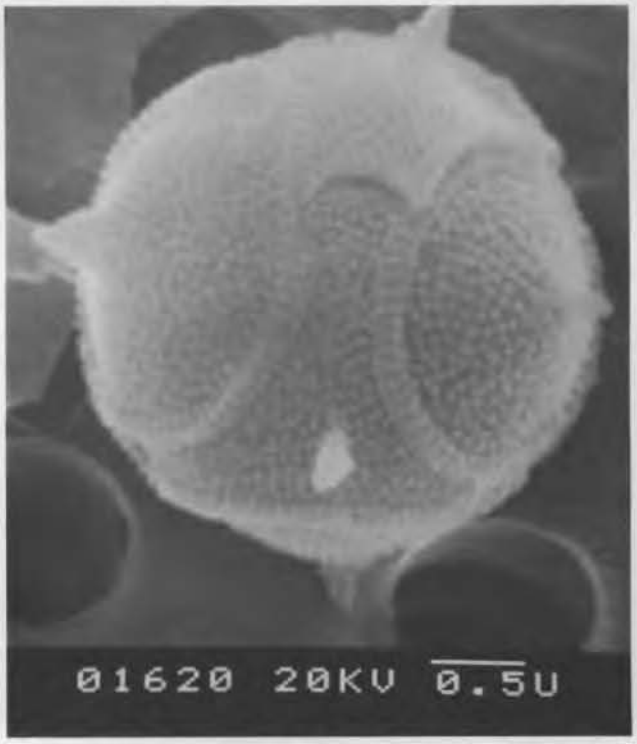

Figure 11. Siliceous cyst no. 9. White bar at bottom = 0.5 μm.

from present-day oceans and were thought to represent unknown or extinct marine chrysophytes. Mitchell and Silver (1982) were the first to report on the occurrence of *A. areolata* and *L. spectabilis*, among others, in their samples from both the water column and the sea ice of the Weddell Sea.

A few choanoflagellate species, *Bicostata spinifera* Throndsen, *Calliacantha simplex* Manton and Oates, and *Diaphanoeca pedicellata* Leadbeater were also seen in several of our samples at concentrations $\geq 10^3$. A siliceous cyst (Fig. 11), identified by several authors (Booth et al. 1980, 1981; Silver et al. 1980) as "siliceous cyst #9", was observed in our ice chunk. It has been suggested by the previously mentioned authors that this cyst is a resting stage in the choanoflagellate life cycle.

Several specimens of a silicoflagellate, *Distephanus speculum* (Ehrenberg) Haeckel (Fig. 12), were observed in the ice chunk and in ice core 22-10/N. Several individuals of an unidentified Gymnodiniaceae were seen in ice core 23-10/N (Table 2). In addition, the colonial form of *Phaeocystis* cf. *pouchetti* was also encountered in both 22- and 23-10/N (Table 2).

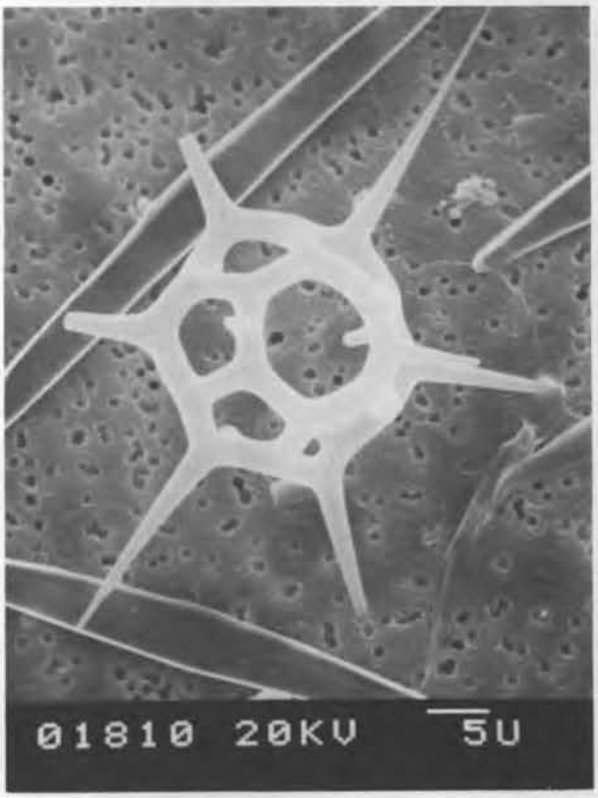

Figure 12. Silicoflagellate: Distephanus speculum. *White bar at bottom = 5 μm.*

DISCUSSION

The downcore changes in relative abundance of the species in 23–10/N and their apparent correlation to the frazil/congelation boundary leads one to wonder whether they are the result of the ice having formed from different water columns or of differential diatom growth in the ice types. Since this core is composed of two different ice types, we know that the frazil ice formed over a period of several hours, while the congelation ice at the bottom undoubtedly formed over the next several weeks. During this time the underlying water column may have changed slightly. Perhaps a warm Weddell Deep Water cell (Gordon and Huber 1983) passed under the ice sheet, changing the biological constituents that were later incorporated into the ice. Three of the species (*N. cylindrus, N. prolongatoides*, and *Ch. dichaeta*) show a marked increase in abundance at and below the frazil/congelation boundary (Fig. 9). This suggests that they were either at higher concentrations in the water when the congelation ice formed or that, once incorporated into the ice, a suitable environment for growth existed. The fact that these same three species were found in high abundance in other cores composed only of frazil ice suggests that the structure alone does not enhance growth. A fourth species, *T. glacialis*, shows the opposite pattern, that is, a decrease in abundance below the frazil/congelation boundary. It is possible that this species was at a lower concentration in the water column when the congelation ice formed or that it has a different optimum light intensity for peak growth than the other three species.

N. prolongatoides was also found in high abundance (14–88%) in several other cores sampled at depth regardless of ice type. *N. closterium* is high (18–48%) in samples from the surface to depth irrespective of structure, while the downcore abundance in 23–10/N shows a bimodal peak, near the surface and near the bottom of the core. Bunt (1964) has demonstrated that certain species are shade-adapted and that variations in light intensity influence productivity. It is possible then that optimal light conditions for *T. glacialis* exist close to the surface while for *N. prolongatoides* conditions are more favorable near the bottom.

Several authors (Bunt 1963, Hoshiai 1977, Sullivan and Palmisano 1981) have reported high chlorophyll *a* concentrations (248–2100 mg/l m^3) in the bottom 20 cm of cores taken in fast (congelation) ice at McMurdo. Clarke and Ackley (in press) have reported an increase in chlorophyll concentrations in frazil ice with depth, but this is not limited to the bottom 20 cm and does not reach the magnitude of other studies (avg. chl *a* in surface frazil ice = 0.46 mg/m^3, frazil ice at depth = 1.36 mg/m^3). This suggests that proximity to the underlying water and thus passive nutrient exchange, which would be greater in congelation ice, might account for the near-bottom abundance peaks of the three species in 23–10/N.

Congelation ice rejects impurities during formation, but frazil ice is capable of mechanically concentrating material, so it is difficult to account for the higher chlorophyll values in the congelation ice cores (0.09–0.42 mg/m^3) relative to the lower values in the surrounding waters (0.07–0.13 mg/m^3) unless growth is occurring.

Buck (personal communication) found isogametes of two of the abundant species in one of the cores he examined, which is indicative of reproduction. In addition, Clarke and Ackley (in press) found that both silicic acid and nitrate concentrations in the ice cores were depleted with regard to the sea-water dilution curve, indicating the assimilation of SiO_4 and NO_3 by diatoms. Therefore, one mechanism to explain the relative differences in species abundances that we see in our samples may be the variation in species concentration in the water column at the time of ice formation. This initial difference appears to be greatly enhanced by subsequent differential growth of species.

Watanabe (1982) has summarized the abundant species present in Antarctic sea ice. To his list we add eight additional species that were abundant (>10%) in Weddell Sea ice (Ackley et al. 1979, Buck and Garrison, in prep.; this paper) (Table 4). Of these eight species, five are pennate forms and two are centrics. Only Bunt and Wood (1963) and Watanabe (1982) have reported diatom communities that are dominated by centric forms. The centric-to-pennate ratio in our samples ranges from 1:6 to 1:34, with an average of 1:16. *Ch. dichaeta* and *Porosira pseudodenticulata* Jouse were present in those samples where centrics were more abundant. The latter is one of the species reported by Watanabe (1982), whereas *Ch. dichaeta* has never been reported as numerically significant in Antarctic sea ice.

We anticipated some correlation between the number of full and empty cells/liter with chlorophyll *a* and phaeophytin ratios, but we did not find one. This may be attributed to the small number of samples (9) for which we have cells/liter data or it may be due to differences in cell volumes. The chlorophyll in a small number of large-volume cells can be equal to that in a large number of small-volume cells.

Table 4. List of dominant diatom species found in Antartic sea ice.

Diatom species	*Reference*	*Year*
Amphipleura rutilance var. *antarctica*	Fukushima and Meguro	1966
Amphiprora kufferathii	Fukushima and Meguro	1966
Amphiprora kjellmanii	Bunt and Wood	1963
Amphiprora oestrupii	Bunt and Wood	1963
Biddulphia weissflogii	Bunt and Wood	1963
Chaetoceros sp. cf. *gracilis*	Ackley et al.	1979
Chaetoceros dichaeta	Clarke et al.	this paper
Coscinodiscus furcatus	Watanabe	1982
Coscinodiscus subtilis	Bunt and Wood	1963
Eucampia antarctica	Bunt and Wood	1963
Navicula glaciei	Richardson and Whitaker	1979
Nitzschia closterium	Ackley et al.	1979
	Clarke et al.	this paper
Nitzschia curta	Burkholder and Mandelli	1965
	Richardson and Whitaker	1979
	Ackley et al.	1979
	Buck and Garrison	in prep.
Nitzschia cylindrus	Ackley et al.	1979
	Clarke et al.	this paper
Nitzschia linearis	Bunt and Wood	1963
Nitzschia martiana	Bunt and Wood	1963
Nitzschia prolongatoides	Clarke et al.	this paper
Nitzschia seriata	Bunt and Wood	1963
Nitzschia stellata	Fukushima and Meguro	1966
Nitzschia subcurvata	Buck and Garrison	in prep
	Clarke et al.	this paper
Nitzschia turgiduloides	Clarke et al.	this paper
Pleurosigma antarctica	Bunt and Wood	1963
Porosira pseudodenticulata	Watanabe	1982
Rhizosolenia alata	Bunt and Wood	1963
Rhizosolenia rostrata	Bunt and Wood	1963
Tropidoneis glacialis	Clarke et al.	this paper

CONCLUSIONS

Diatoms are found throughout the length of the ice cores, although relative species abundances fluctuated downcore. Pennate forms were numerically dominant over centrics. Three of the species previously reported as being abundant in Antarctic ice (*N. closterium, N. cylindrus,* and *N. subcurvata*) were also abundant in our samples. Four additional species (*Ch. dichaeta, N. prolongatoides, N. turgiduloides,* and *T. glacialis*) not previously reported were found to be numerically dominant. Comparison of the size ranges reported in the literature with our measurements shows that, particularly among the *Nitzchia* species, our specimens were often smaller than those previously reported from the water column. Full diatom cells are generally 10 times more abundant than empty cells. In 23-10/N, examined at 10-cm intervals, the peaks of the most abundant species were, in all but one instance, due to a sharp increase in the number of full cells/liter, without a concomitant increase in empty cells/liter.

Differences in species abundances are attributed initially to incorporation of biological material at different times from slightly different water columns. Subsequent growth within the ice, which is affected by differences in light intensity, ice structure, and proximity to nutrients in the underlying water, changes the original species abundances.

LITERATURE CITED

Ackley, S.F. (1982) Ice scavenging and nucleation: Two mechanisms for incorporation of algae into newly forming sea ice. *EOS, Transactions of the American Geophysical Union,* **63**(3), p. 47.

Ackley, S.F., K.R. Buck and S. Taguchi (1979) Standing crop of algae in the sea ice of the Weddell region. *Deep Sea Research,* **26A:** 269-281.

Ackley, S.F., D.B. Clarke and S.J. Smitt. (1983) Physical, chemical and biological properties of sea ice cores. Reports of the U.S.-U.S.S.R. Weddell Polynya Expedition, October-November 1981, Vol. 4. USA Cold Regions Research and Engi-

neering Laboratory, Technical Note, 30 pp. (unpublished).

Booth, B.C., J. Lewin and R.E. Norris (1980) Siliceous Nanoplankton. I. Newly discovered cysts from the Gulf of Alaska. *Marine Biology,* **58:** 205–209.

Buck, K.R. and D.L. Garrison (In prep.) Protists from the water column at the Weddell Sea ice edge. (Submitted to *Deep Sea Research.*)

Bunt, J.S. (1963) Diatoms of Antarctic sea ice as agents of primary production. *Nature,* **199:** 1255–1257.

Bunt, J.S. (1964) Primary production under sea ice in Antarctic water. 2. Influence of light and other factors on photosynthetic activities of Antarctic marine microalgae. In *Biology of Antarctic Seas Antarctic Research Series* (M.O. Lee, Ed.), **1:** 27-31.

Bunt, J.S. and E.J.F. Wood (1963) Microalgae and Antarctic sea ice. *Nature,* **199:** 1254–1255.

Burkholder, P.R. and E.F. Mandelli (1965) Productivity of microalgae in Antarctic sea ice. *Science,* **149**(3686): 872–874.

Buynitsky, V.Kh. (1977) Organic life in sea ice. In *Polar Oceans* (M.J. Dunbar, Ed.). Arctic Institute of North America, p. 301–306.

Clarke, D.B. and S.F. Ackley (1982) Physical, chemical and biological properties of winter sea ice in the Weddell Sea. *Antarctic Journal of the U.S.,* **17**(5): 107-108.

Clarke, D.B. and S.F. Ackley (In press) Sea ice structure and biological activity in the Antarctic marginal ice zone. *Journal of Geophysical Research.*

Evenson, D.E. and G.R. Hasle (1975) The morphology of some *Chaetoceros* species as seen in the electron microscopes. *Nova Hedwigia•Beiheft,* **53:** 153–169.

Fenner, J., H.J. Schrader and H. Wienigk (1976) III Diatom phytoplankton studies in the Southern Pacific Ocean, composition and correlation to the Antarctic convergence and its paleoecological significance. In *Initial Reports of the Deep Sea Drilling Project,* Washington, D.C. (U.S. Government Printing Office), **35:** 757–813.

Fryxell, G.A. (1977) *Thalassiosira australis* Peragallo and *T. lentiginosa* (Janisch) G. Fryxell, comb. nov.: two Antarctic diatoms (Bacillariophyceae). *Phycologia,* **16**(1): 95–104.

Fryxell, G.A. and G.R. Hasle (1979a) The genus *Thalassiosira: T. trifulta* sp. nova and other species with tricolumnar supports on strutted processes. *Nova Hedwigia•Beiheft,* **64:** 13–40.

Fryxell, G.A. and G.R. Hasle (1979b) The genus *Thalassiosira:* species with internal extensions of the strutted processes. *Phycologia,* **18**(4):378–393.

Fryxell, G.A. and G.R. Hasle (In press) The Antarctic diatoms: *Thalassiosira dichotomica* (Kozlova) comb. nov. and *T. ambigua* Kozlova. *Polar Biology.*

Fukushima, H. and H. Meguro (1966) The plankton ice as basic factor of the primary production in the Antarctic Ocean. *Antarctic Record,* **27:** 99–101.

Garrison, D.L. and K.R. Buck (In prep.) Sea-ice algae in the Weddell Sea. I. Algal biomass and nutrients in sea ice. (Submitted to *Deep Sea Research.*)

Garrison, D.L., S.F. Ackley and K.R. Buck (1983) A physical mechanism for establishing algal populations in frazil ice. *Nature,* **306**(5491): 363-365.

Gordon, A.L. and E.I. Sarukhanyan (1982) American and Soviet expedition into the Southern Ocean sea ice in October and November 1981. *EOS, Transactions of the American Geophysical Union,* **63**(1): 2.

Gordon, A.L. and B.A. Huber (in prep.) Thermohaline stratification below the Southern Ocean sea ice. (Submitted to *Journal of Geophysical Research.*)

Gow, A.J., S.F. Ackley, W.F. Weeks and J.W. Govoni (1982) Physical and structural characteristics of Antarctic sea ice. *Annals of Glaciology,* **3:** 113–117.

Hasle, G.R. (1964) *Nitzschia* and *Fragilariopsis* species studied in the light and electron microscopes. I. Some marine species of the groups Nitzschiella and Lanceolatae. *Skrifter Norske Videnskaps-Akademi i Oslo. Mat.-Naturv. Kl., N.S.* **16:** 1–48.

Hasle, G.R. (1965a) *Nitzschia* and *Fragilariopsis* species studied in the light and electron microscopes. II. The group Pseudonitzschia. *Skrifter Norske Videnskaps-Akademi i Oslo. Mat.-Naturv. Kl., N.S.* **18:** 1–45.

Hasle, G.R. (1965b) *Nitzschia* and *Fragilariopsis* species studied in the light and electron microscopes. III. The genus *Fragilariopsis. Skrifter Norske Videnskaps-Akademi i Oslo. Mat.-Naturv. Kl., N.S.* **21:** 1–49.

Hasle, G.R. (1968) Observations on the marine diatom *Fragilariopsis kerguelensis* (O'Meara) Hust. in the scanning electron microscope. *Nytt Magasin for Botanik,* **15:** 205–208.

Hasle, G.R. (1973) Some marine plankton genera of the diatom family Thalassiosiraceae. *Nova Hedwigia•Beiheft,* **45:** 1–49.

Hasle, G.R. (1975) Some living marine species of the diatom family Rhizosoleniaceae. *Nova Hedwigia•Beiheft,* pp. 99–140.

Hasle, G.R. and B.R. Heimdal (1970) Some species of the centric diatom genus *Thalassiosira* studied in the light and electron microscopes. *Nova Hedwigia•Beiheft,* **31:** 543–581.

Hendy, N.I. (1937) The planktonic diatoms of the Southern Seas. *Discovery Report,* **16:** 151–364.

Hoshiai, T. (1977) Seasonal change of ice communities in the sea ice near Syowa Station, Antarctica. In *Polar Oceans* (M.J. Dunbar, Ed.), *Arctic Institute of North America,* pp. 307–317.

Manguin, E. (1960) Les diatomées de la Terre Adélie campagne du "Commandant Charcot" 1949–1950. *Annals of Natural Science, Botany,* 12th Series.

Meguro, H. (1962) Plankton ice in the Antarctic Ocean. *Antarctic Record,* **14:** 72–79.

Meguro, H., K. Ito and H. Fukushima (1967) Ice flora (bottom type): A mechanism of primary production in polar seas and the growth of diatoms in sea ice. *Arctic,* **20:** 114–133.

Mitchell, J.G. and M.W. Silver (1982) Modern archaeomonads indicate sea-ice environments. *Nature,* **296**(5856): 437–439.

Richardson, M.G. and T.M. Whitaker (1979) An Antarctic fast-ice food chain: Observations on the interaction of the amphipod *Pontogoneia antarctica* Chevereux with ice-associated microalgae. *British Antarctic Survey Bulletin,* **47:** 107–115.

Silver, M.W., J.G. Mitchell and D.L. Ringo (1980) Siliceous nanoplankton. II. Newly discovered cysts and abundant Choanoflagellates from the Weddell Sea, Antarctica. *Marine Biology,* **58:** 211–217.

Sullivan, C.W. and A.C. Palmisano (1981) Sea ice microbial communities in McMurdo Sound. *Antarctic Journal of the U.S.,* **16**(5): 126–127.

Syvertsen, E.E. (1977) *Thalassiosira rotula* and *T. gravida:* Ecology and Morphology. In *Fourth Symposium on Recent and Fossil Marine Diatoms.* (R. Simorisen, Ed.), J. Cramer (Publ.), Germany.

Watanabe, K. (1982) Centric diatom communities found in the Antarctic sea ice. *Antarctic Record,* **74:** 119–126.

Weeks, W.F. and S.F. Ackley (1982) The growth, structure and properties of sea ice. USA Cold Regions Research and Engineering Laboratory, CRREL Monograph 82-1, ADA123762.

APPENDIX A: TAXONOMIC TERMS

Areolae	Regularly repeated perforations (polygonal or rounded) through the basal siliceous layer, normally occluded by a velum.
Apical axis	Longitudinal axis of a valve.
Arcuate	Arched or bow shaped.
Canal raphe	Raphe with a tubular passage running along its inner side, separated from the rest of the interior of the frustule by the fibulae (keel puncta); the spaces between are called interspaces.
Central nodule	A thickened area between the two central pores of the raphe.
Cingulum	The portion of the girdle associated with a single valve.
Copula	One of three elements of the cingulum, it is a band between the valvocopula and the pleurae. Often but not always areolate; less ornate than the valvocopula.
Connecting band	Element of the cingulum distal to the copula or any element when no intercalary bands are present.
Costae	Ribs, elongated solid thickenings of the valve.
Cribrum	A velum perforated by regularly arranged pores.
Dentate	Toothed; the teeth, if spine-like, are very short.
Epitheca	The upper and therefore older half of a frustule; fits over the hypotheca.
Foramen	The passage through the constriction in the valve wall that is opposite the velum.
Frustule	The cell wall of a diatom, composed of two valves (epitheca and hypotheca).
Granule	A small rounded projection on the surface of the valve, a type of spine.
Girdle	Part of the frustule composed of the cingulum (intercalary or connecting bands).
Girdle view	Side view of a diatom, with the overlapping halves (valves) of the frustule apparent, the girdle uppermost in optical view.
Hyaline	An area where the basal siliceous layer is not penetrated by areolae or puncta.
Hypotheca	The lower and younger half of the frustule, within the epitheca.
Infundibulum	A funnel-shaped body that is the internal termination of the raphe.
Intercalary band	An element of the cingulum proximal to the valve, different in structure or form from distal elements.
Keel	In those pennate forms whose valve is sharply angled at the raphe, the summit of the ridge bearing the raphe.
Keel puncta	Pores, or membranes appearing as pores, in the plate lying below the canal raphe.
Labiate process	A tube or opening through the valve wall with an internal flattened tube or longitudinal slit usually surrounded by two lips.
Lanceolate	Lance-shaped, long and narrow with subparallel margins, tapering at the axis.
Ligula	Extension of a girdle band that completely fills in the gap of the opening of the adjacent band. It points toward the valve to which it is attached.
Linear	Long and narrow with parallel sides.
Mantle	The outermost part of the valve that is apparent in girdle view, but excluding the girdle bands.
Pleurae	One of three elements of the cingulum, the pleurae are bands proximal to the copula and are usually hyaline.
Pseudonodulus	A marginal-submarginal structure set off from the pattern of the rest of the valve structure.

Puncta	Minute pores, valve markings usually in rows (striae).
Raphe	An elongated fissure or pair of fissures through the valve wall (along the main axis).
Setae	Hollow outgrowths of the valve projecting outside the valve margin, with a different structure from the valve.
Spine	A closed or solid structure projecting out from the valve wall.
Stria	Parallel lines of rows of areolae or puncta so crowded as to appear as a solid line.
Strutted process	A tube through the valve wall surrounded by 2–5 chambers or pores separated internally by arched supports, often with threads extruded from the exterior part.
Terminal nodule	A thickened area at the apical end of the valve where the raphe terminates.
Terminal pore	An expansion of the raphe at the apical end.
Transapical axis	The transverse axis of the valve.
Truncate	Having the ends square or even.
Valve	One of two overlapping halves of a frustule.
Valvocopula	One of three elements of the cingulum; a band proximal to the valve, usually ornately areolate.
Velum	A thin and perforate layer of silica across an areola (cribrum, rota, or vola are three types).

APPENDIX B: DIFFERENCES IN SPECIES COMPOSITION AND ABUNDANCE IN DUPLICATE SAMPLES EXAMINED UNDER OPTICAL AND INVERTED LIGHT MICROSCOPES

In the past, numerous techniques have been employed to prepare diatoms for microscopic examination. The choice of preparation technique and the type of microscope used is dependent on one's goals: to study morphologic characteristics and taxonomic relationships or to determine relative or absolute species abundances. The SEM, for example, is the optimal tool to study morphology, as it provides the highest resolution of surface detail and gives a three-dimensional view of the valve. Both the optical and the inverted light microscopes may be used for diatom enumeration, since their resolution is usually adequate to identify most species. But while the optical light microscope can only provide relative abundance due to the sample preparation, the inverted light microscope yields absolute abundance. In addition, it allows one to differentiate between full and empty cells; that is, whether the organic material is still intact.

We prepared five duplicate composite samples for examination under both Leitz (optical) and Zeiss (inverted) microscopes, using the appropriate preparation techniques for each as described in the Materials and Methods section. Our aim was to determine how preparation techniques might change the species compositions.

In all of the samples the majority of the species were the same, with a few species observed under one microscope and not the other. However, two species that occurred in abundance, *Nitzschia prolongatoides* (76%) and *Dactyliosolen antarcticus* (0–23%), were consistently observed under the inverted microscope but never under the optical microscope. Three additional species, *N. closterium* (29%), *N. subcurvata* (0.8–15%) and *Ch. dichaeta* (0.6–14%), were common in several samples examined under the inverted microscope but were not seen in the same sample under the optical microscope. They were however, observed in other optical microscope samples. A few species were seen under the optical microscope but not under the inverted microscope, but these generally accounted for less than 3% except in the case of *N. curta* and *N. cylindrus*, which were higher. For these two species, optical microscope counts were considerably higher than the inverted microscope counts in three of the samples (37–65% optical, 1–2% inverted).

A possible explanation for the higher optical microscope counts of *N. curta* and *N. cylindrus* in these three samples is that, having lost (through preparation) the original dominant species (*N. prolongatoides*), these two now assume disproportionate significance. The fact that they are found in equal numbers in the other two samples, which do not have *N. prolongatoides*, might seem to substantiate this.

We do not believe any of these discrepancies are artifacts of the optical microscope, but rather that they result from the preparation technique employed. Species not observed under the optical microscope may have been selectively eliminated during sample preparation. Several steps are involved that could conceivably lead to loss of material. Therefore we conclude that the inverted microscope, which only requires that a sample be thawed, agitated, and then settled overnight, is the better method for diatom enumeration from sea ice and water column samples.

APPENDIX C: MORPHOLOGIC DESCRIPTIONS AND SEM MICROGRAPHS

All SEM micrographs have a white bar in the lower right hand corner. The length of this line usually represents 5 μm, but may be 0.5 or 50 μm, as indicated below the line. The typical view of the diatom valve/frustule represented is an exterior valve view. Interior, girdle, or oblique views are indicated in the figure caption.

Asteromphalus hyalinus Karsten

The valves are convex with a diameter of 16 to 26 μm. There are 4 or 5 hyaline rays consisting of elongated chambers that open to the interior in long radial slits and terminate on the exterior in a pseudonodulus (Fig. C1a). The rays are 2-3 μm wide and are curved, with the exception of one that is straight and narrow. On the marginal side of each ray, there is a large curved labiate process that extends a short distance into the interior (Fig. C1b). The central area is eccentric, and its diameter is approximately one-half of the total valve diameter. There are 9 to 13 areolae in 10 μm (Fenner et al. 1976). The cribrum is external and the foramen is internal.

a) Valve showing curved hyaline rays, pseudonodulus (large arrow), external opening of labiate process (thin arrow), and cribrum.

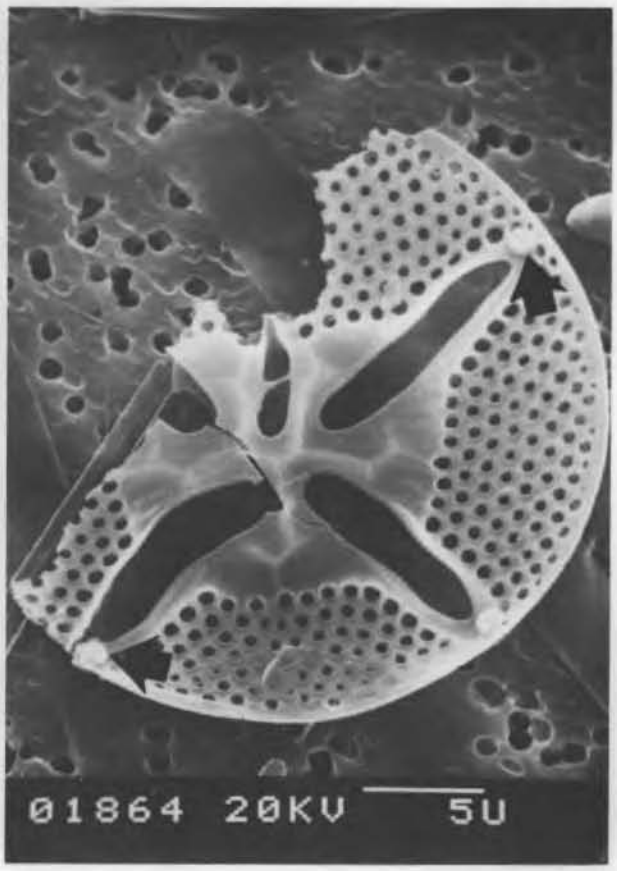

b) Valve (interior) showing hyaline rays, foramen, and labiate processes on the marginal side of each ray (arrow).

Figure C1. Asteromphalus hyalinus.

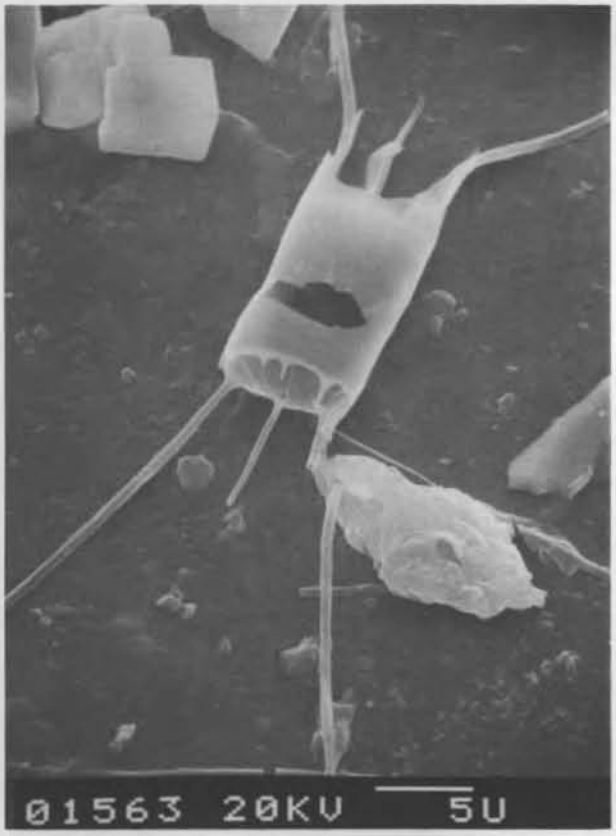

a) Rectangular frustule (girdle view) showing central labiate process and curved setae. Valve has a hole in the region of the girdle bands.

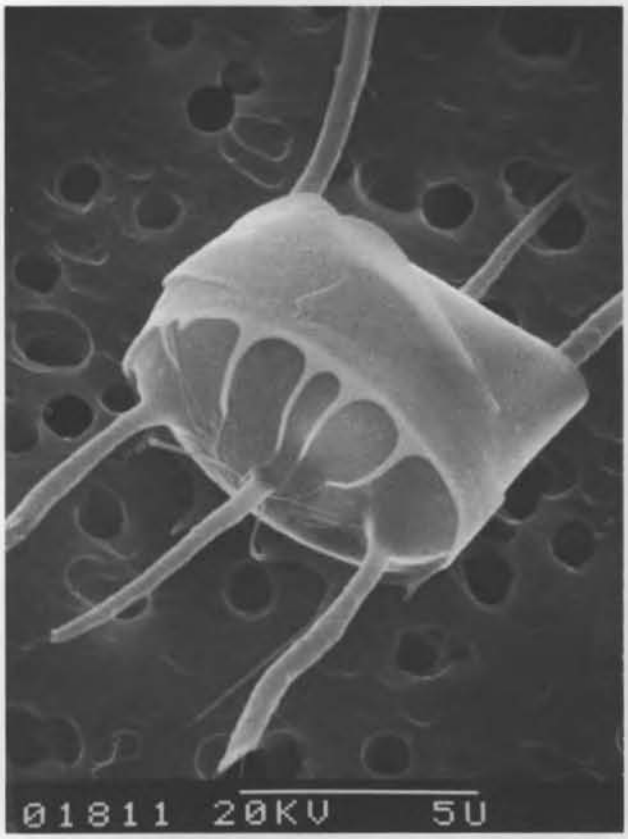

b) Spherical frustule (girdle view). Central labiate process is evident and setae are broken.

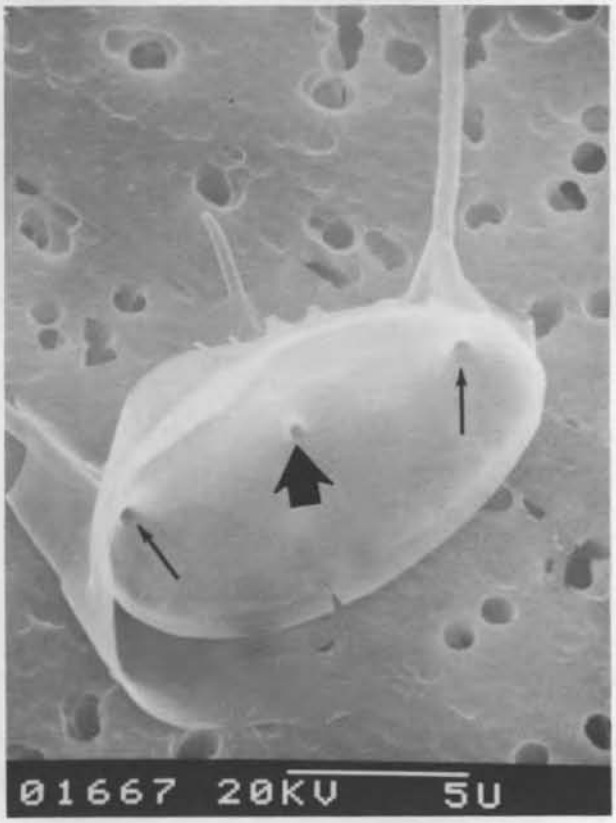

c) Valve (interior, oblique view) showing the openings to the hollow labiate process (large arrow) and hollow setae (thin arrow).

Figure C2. Chaetoceros dichaeta.

Chaetoceros dichaeta Ehrenberg

This species typically occurs in straight chains composed of several individuals. The cells vary from rectangular (Fig. C2a) to spherical (Fig. C2b) in shape. Length along the apical axis ranges from 10 to 47 μm (Manguin 1960). About 10–20 μm above the valve, the setae bend abruptly at a right angle and cross those of the adjacent valve. The setae are circular in cross section with small spines (Evenson and Hasle 1975). They are the same diameter for most of their length but thin slightly at the extremities. Both the setae and the long central labiate process are hollow, which can be seen in the interior view shown in (Fig. C2c).

Chaetoceros neglectum Karsten

This species occurs in flexible chains of weakly silicified rectangular cells (Fig. C3a). Perivalvar axis height is between 5.5 and 7 μm, and the length along the apical axis is 8.5 to 9 μm (Manguin 1960). The setae are delicate and smooth, curving above the valve and running perpendicular to the axis of the valve. Setae of adjoining cells are fused at the curve (Fig. C3b). There is no labiate process.

Dactyliosolen antarcticus Castracane

The diameter of the valves varies from 13 to 90 μm. There are 2–3 intercalary bands in 10 μm with 2–6 perivalvar ribs in 10 μm. The density of perivalvar ribs can vary from 4 to 15 in 10 μm within a single frustule (Hasle 1975). Each intercalary band consists of two halves, and the interlocking of these half bands forms a distinct oblique line. The valve wall is delicate and has internal costae that converge from the valve margin

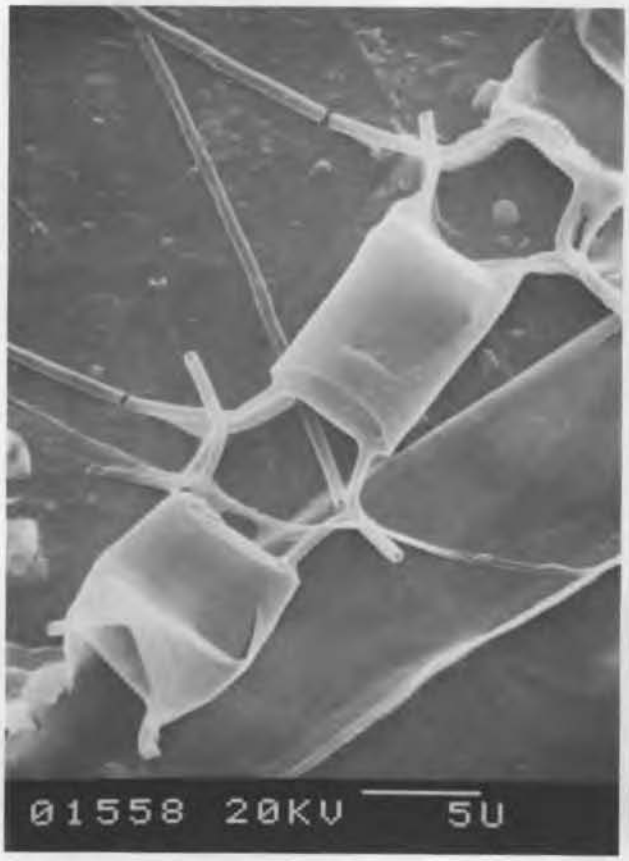

a) Chain of frustules (girdle view) showing rectangular valve outline and smooth curved setae.

b) Frustule (girdle view) and adjoining lower valve showing fused setae (arrow).

Figure C3. Chaetoceros neglectum.

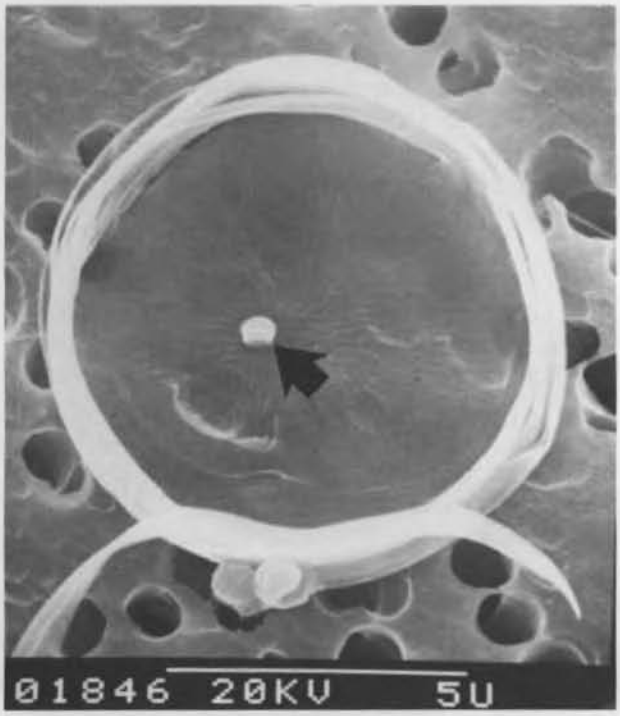

a) Valve with attached girdle bands (interior) showing undulating, branched costae and labiate process slightly off center (arrow).

b) Broken frustule (oblique view) showing hole of labiate process (large arrow), small granules (thin arrow), and areolate girdle bands.

Figure C4. Dactyliosolen antarcticus.

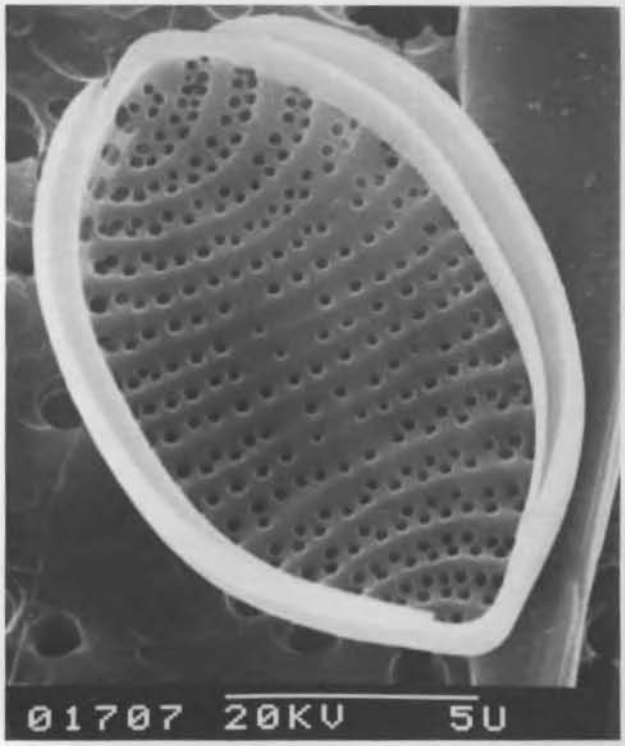

a) Valve with attached girdle band (interior). Costae and poroids are evident.

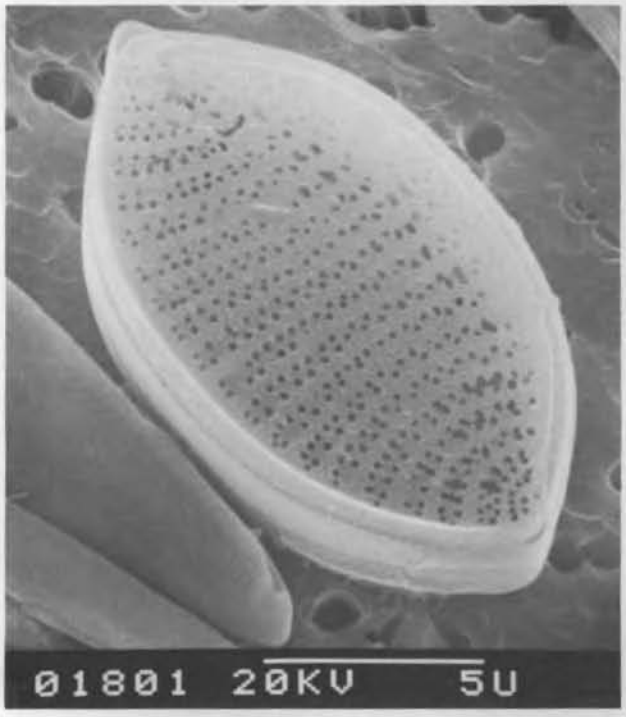

b) Complete frustule with some poroids dissolving into each other. Upper valve is cracked at apical end.

Figure C5. Nitzschia angulata.

toward a labiate process (Fig. C4a). The costae are straight on the shallow valve mantle but undulate and are branched over most of the valve face. A row of small granules can be seen in Figure C4b on the valve mantle. While the labiate process is usually located near the margin, it may occasionally be near the center. It has no external extension, but internally it has a typical labiate shape.

Nitzschia angulata Hasle

This species has a variable valve outline; the smallest specimens are circular to elliptical and the largest are lanceolate. Hasle (1965b) reported it to be 8–53 μm long and 7–13 μm wide, with 8–16 transapical costae in 10 μm. The specimens we measured were 13–16 μm long and 7–7.5 μm wide. The transapical costae are straight in the middle and curved at the ends. The intercostal membrane is perforated by two rows of alternating poroids, 22–26 in 10 μm (Hasle 1965b). Figure C5a shows an exterior and Figure C5b an interior valve view.

Nitzschia closterium (Ehrenberg) W. Smith

This species is not well documented in our SEM micrographs, as it is delicate and weakly silicified and hence whole halves were not often observed. Figure C6 shows a typical valve. The range of variation in shape that we observed, from straight to sigmoid-shaped cells with either straight or curved rostra, is typical and has previously been noted in the literature. However, while Hasle (1964) found the largest specimens in the Antarctic (< 400 μm long) with a mean range of 125–150 μm, our largest specimen was 190 μm and our range 70 to 190 μm.

Figure C6. Nitzschia closterium. *Valve showing inflated cell body (arrow) and delicate curved rostra.*

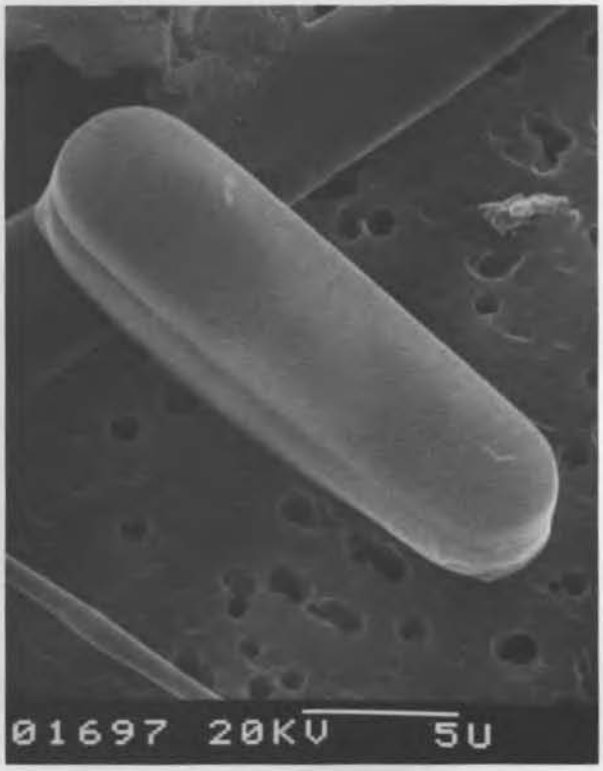

a) Frustule (oblique view); heteropole axis is evident.

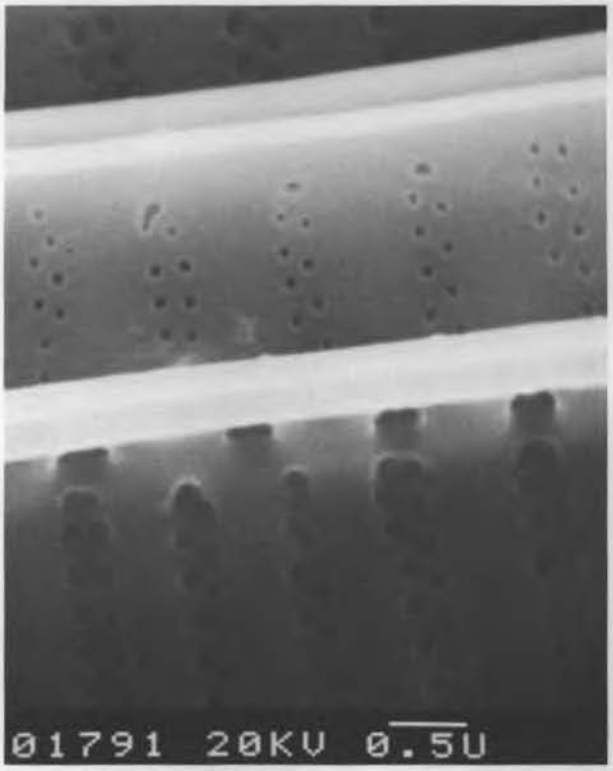

b) Closeup of three valves (top to bottom: interior, exterior, interior) with costae, double rows of poroids, and keel puncta (on bottom valve) evident.

Figure C7. Nitzschia curta.

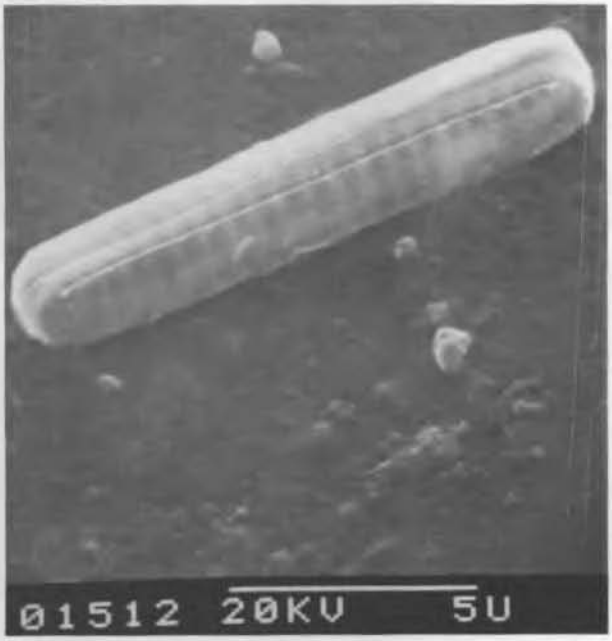

Figure C8. Nitzschia cylindrus. *Frustule (oblique view) with costae, keel, and raphe visible.*

Nitzschia curta (Van Heurck) Hasle and *N. cylindrus* (Grunow) Hasle

These two species exhibit an overlap in both their size range and the number of rows of poroids. The most easily distinguished characteristic is the heteropolarity of *N. curta* as seen in Figure C7a, which shows that one pole is broader than the other. In comparison, the isopolarity of *N. cylindrus* can be seen in Figure C8, which clearly shows the straight parallel margins and the broadly rounded apices. In addition, *N. curta* is characterized by straight transapical costae over most of the valve with those near the poles being curved. Hasle (1965b) reported the length as 10–42 μm, and the width as 3.5–6 μm, with 9–12 costae in 10 μm. We found several smaller individuals and none as large as Hasle's. Our size range was 5.5–29 μm long and 0.8–5 μm wide. Double rows of poroids are situated close to the costae and usually occur at a frequency of 30 in 10 μm (Hasle 1965b). Figure C7b shows the double rows of poroids as seen from both the interior and exterior. The straight transapical costae of *N. cylindrus*

are confined to the rectangular portion of the valve, with more weakly silicified oblique or longitudinal costae at the ends. Hasle (1965b) reported *N. cylindrus*'s length as 6–40 μm and the width as 2–4 μm, with 13–17 transapical costae in 10 μm. As with *N. curta*, we found some specimens smaller than Hasle reported and none quite so large. Our size range was 3.5–15 μm long and 1.25–4 μm wide. There were 5–8 poroids perforating the intercostal membranes in 1 μm, arranged in 2 to 4 transapical rows (Hasle 1965b).

Nitzschia kerguelensis (O'Meara) Hasle

Frustules of this species are strongly silicified and coarsely structured. The transapical ribs are straight except near the poles, where they curve slightly. The thick-walled intercostal membrane is punctate with two rows of alternating poroids (8–10 in 10 μm). The keel puncta are not as easily distinguished as in other *Nitzschia* species (Hasle 1968). Hasle (1965b) reports lengths of 10–76 μm and widths of 5–11 μm. Some of our specimens were smaller and none so large: length, 6.5–28.5 μm, and width, 3–11 μm. This species is easily recognized in girdle view due its coarse striations. Figure C9a of a valve at an oblique angle shows both the valve face and girdle. Figure C9b is an interior valve view showing the robust costae and double rows of poroids.

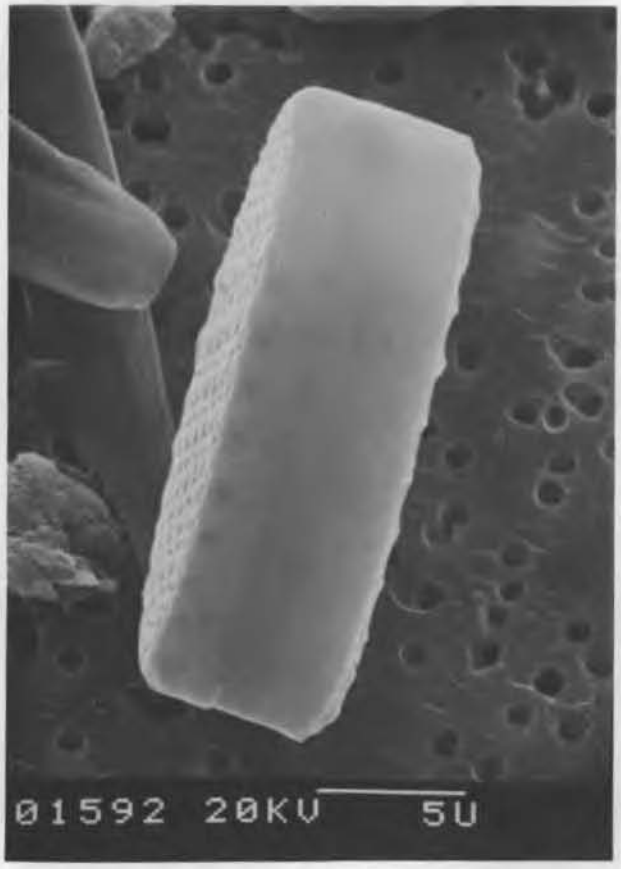

a) Frustule (oblique, girdle view). Robust costae and double rows of poroids; and girdle bands are visible.

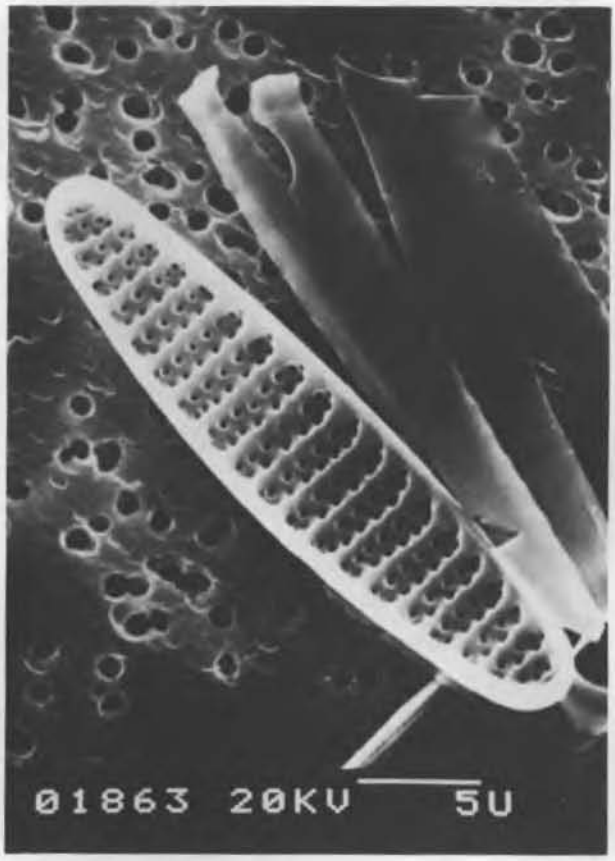

b) Valve (interior) with costae and poroids evident.

Figure C9. Nitzschia kerguelensis.

Nitzschia prolongatoides Hasle

This species occurred in low abundance in the samples examined under the SEM, so we have only one photo. Figure C10 shows the characteristic valve outline with slightly enlarged ends. This specimen measured 50 μm long and 1 μm wide, which is within the size range given by Hasle (1965a) (length, 20–70 μm; width 0.5–2.5 μm).

Nitzschia ritscheri (Hustedt) Hasle

The valve outline of this species varies with the size of the individual. Small specimens are linear to elliptical with broadly rounded poles. Large specimens are linear to lanceolate with a heteropole apical axis, rounded at the broad pole and tapering at the narrow. Costae adjacent to the broad pole are more oblique than those near the narrow pole. Poroids (18–24 in 10 μm) are arranged in two rows (Hasle 1965b). Figure C11 shows a slightly heteropole individual.

Nitzschia subcurvata Hasle

This species has valves that are narrow, dilated in the middle, and abruptly attenuated towards long slender rostra. The apical axis is curved in the transapical direction. One side of the valve is straight or slightly concave, and the other side is convex, especially in the middle of the valve. This can be seen in Figure C12a, an interior view of two frustules. Hasle (1964) recorded lengths of 47–90 μm and widths of 1.5–2 μm. Our specimens were comparable: length, 45–60 μm, and width, 1–1.5 μm. The transapical costae (44–49 in 10 μm) are not resolvable under a light microscope (Hasle 1964). The intercostal membrane, perforated by one row of poroids (50 in 10 μm), and the keel puncta can be seen in Figure C12b.

Nitzschia turgiduloides Hasle

This species has parallel sides with broadly rounded apices. Usually the valve is slightly enlarged in the middle. According to Hasle (1965a), the length is 63–126 μm, and the width at the ends is 1.2–18 μm and 1.8–2.7 μm in the middle. Our specimens measured 73–115 μm long and 1–2 μm wide near the ends, which falls within her size range. Figure C13a shows the valve exterior. Figure C13b, a closeup of the interior, shows the arcuate keel puncta (10–13 in 10 μm), transapical costae (17–21 in 10 μm), and intercostal membrane, which is perforated by 1 or 2 rows of small poroids (8–10 in 1 μm) (Hasle 1965a).

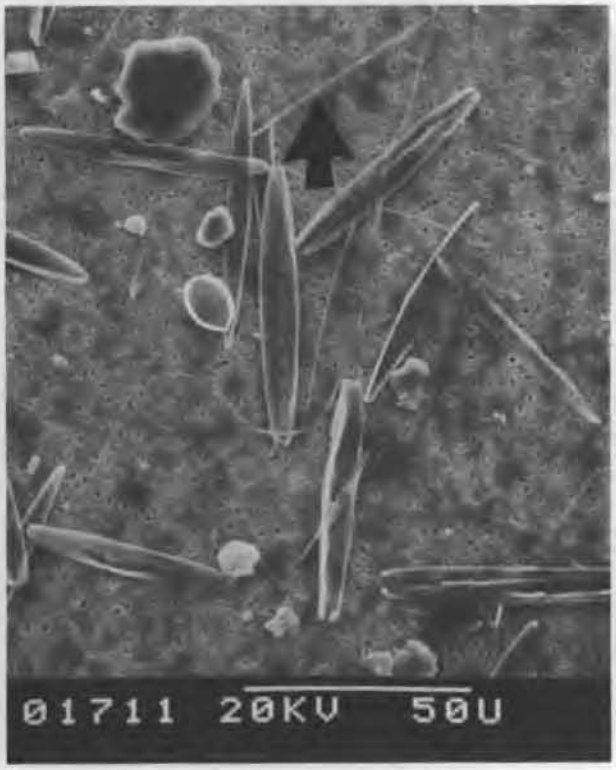

Figure C10. Nitzschia prolongatoides. *Single valve (arrow).*

Figure C11. Nitzschia ritscheri. *Valve with attached girdle bands. Pattern of costae and double rows of poroids are evident.*

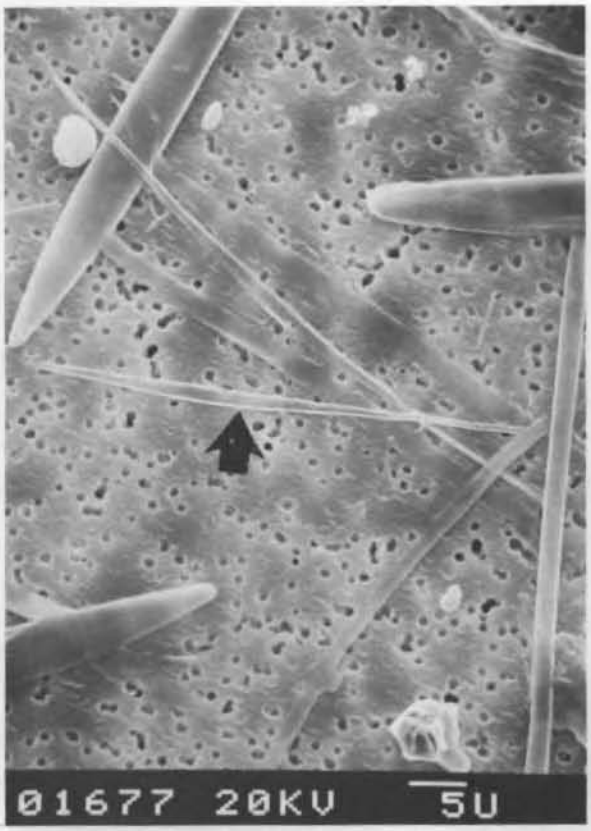

a) Two valves (arrow points to one) (interior).

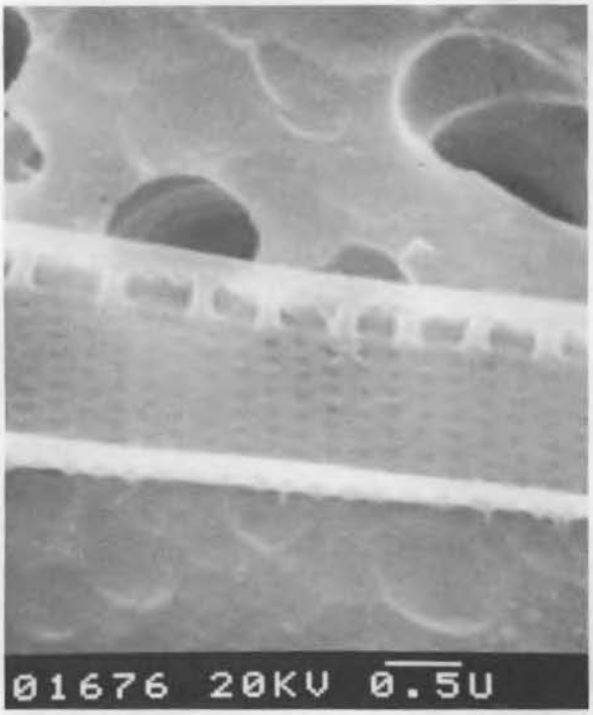

b) Closeup of same valve. Poroids and keel puncta can be seen.

Figure C12. Nitzschia subcurvata.

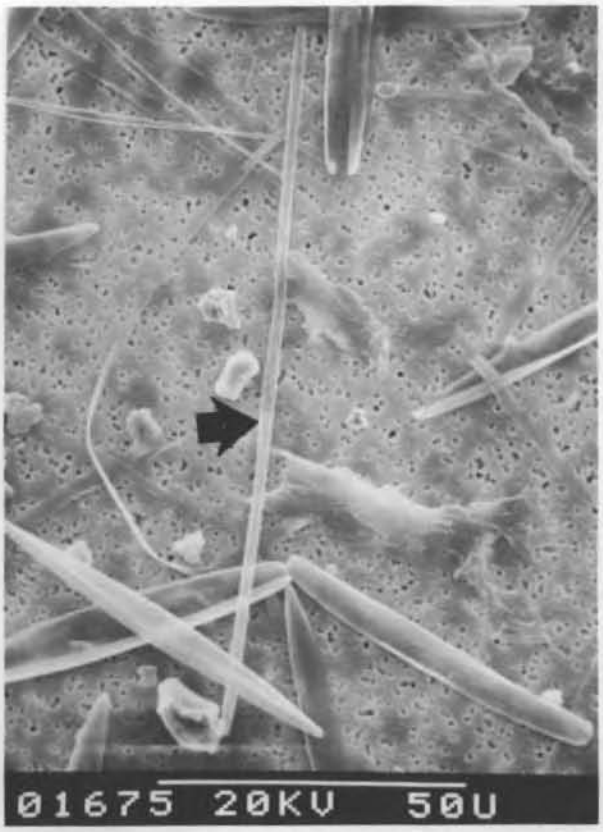

a) Arrow points to valve having characteristic outline with a bulge near the middle.

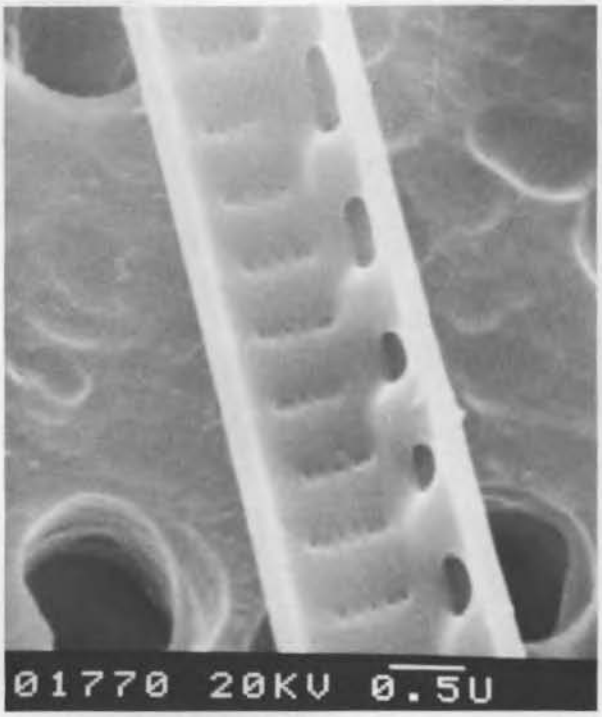

b) Closeup of valve (interior) with costae, single row of poroids, and arcuate keel puncta evident.

Figure C13. Nitzschia turgiduloides.

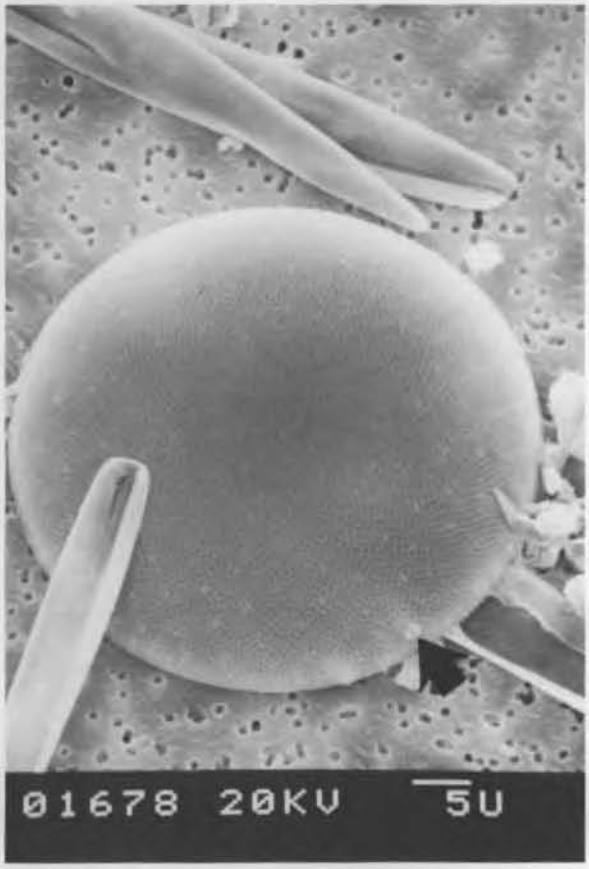

a) Valve showing pattern of areolation and labiate process (arrow).

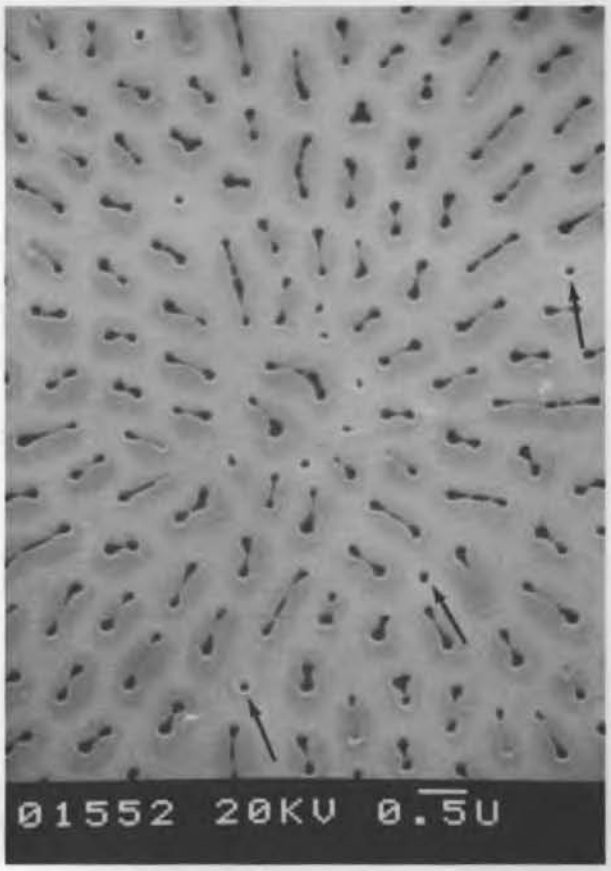

b) Closeup of valve showing areolae, which are elongated but constricted in the middle, and strutted processes (arrows).

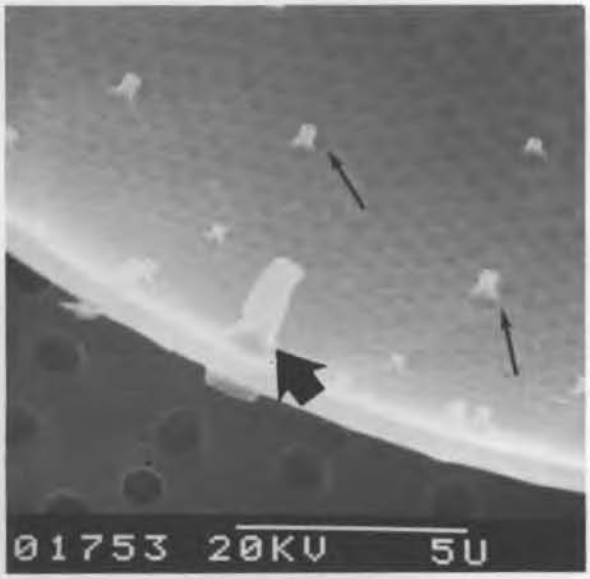

c) Closeup of valve (interior) showing cribrum, strutted processes (thin arrows), and labiate process (large arrow).

Figure C14. Porosira pseudodenticulata.

Porosira pseudodenticulata (Hustedt) Jousé

This is a coarsely silicified species 60 to 80 μm in diameter with 10–12 areolae in 10 μm (Hasle 1973). Some of our specimens were smaller, ranging from 33 to 52 μm. The areolae are arranged in straight, radial rows with secondary irregular spiral rows (Fig. C14a). The shape of the areolae is distinctive, being either elongated and constricted in the middle or tripartite (Fig. C14b). They have a cribrum on the inner valve surface, which can be seen in Figure C14c. Strutted processes are scattered over the valve surface, but they are more numerous in the marginal zone than at the valve center (Fig. C14d). Figure C14c shows an interior and Figure C14e an exterior view of the strutted processes and the single labiate process close to the margin. Externally the strutted processes appear as circular holes with thickened edges, while internally they are fairly short, surrounded by two or three pores. Either internally or externally, the labiate process does not project much above the basal siliceous layer.

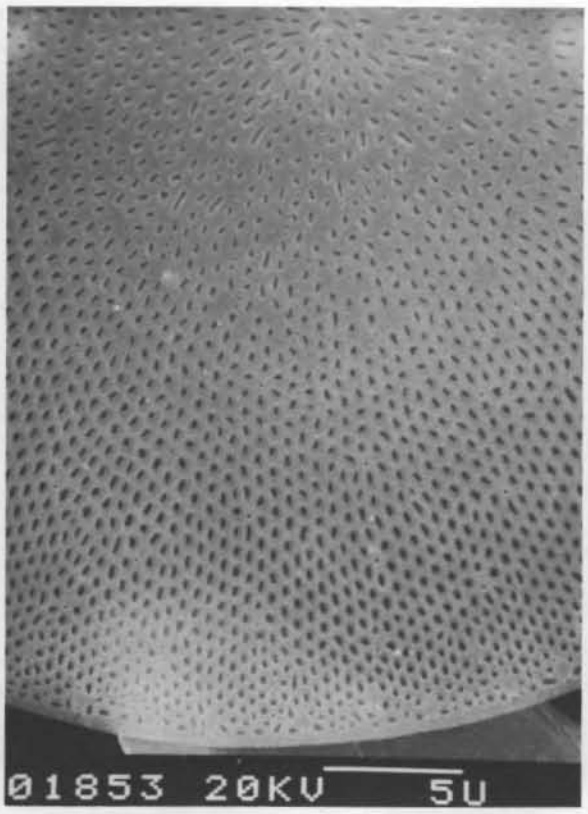

d) Valve showing numerous strutted processes at the margin and fewer at the center.

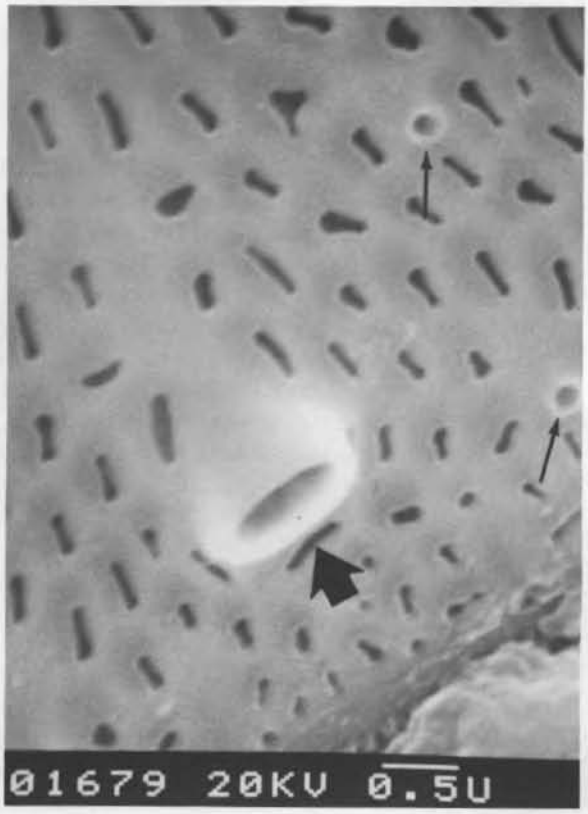

e) Closeup showing the large labiate (large arrow) and strutted processes (thin arrows).

Figure C14 (cont'd).

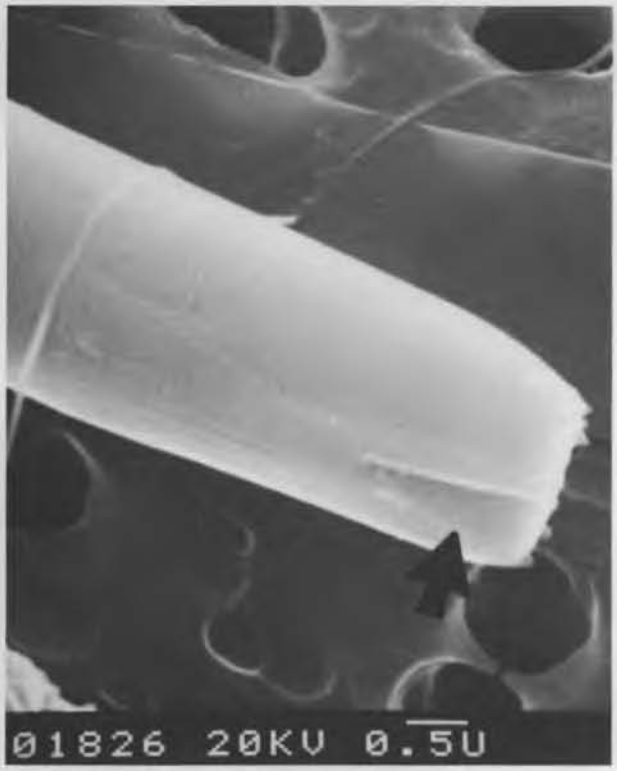

a) Upper part of valve (girdle view), dentate, with longitudinal slit (arrow) and fine areolation.

b) Upper part of valve (girdle view) showing homogeneously silicified ridge (arrow) with depression for contiguous cell.

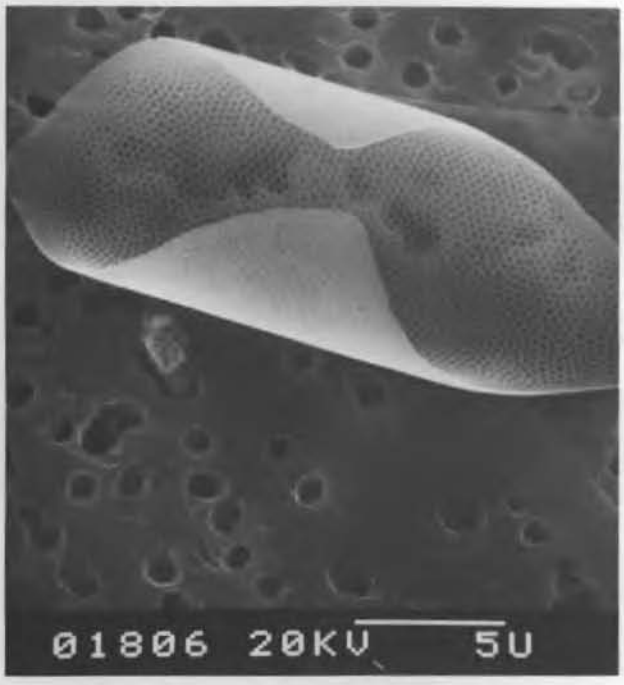

c) Part of band (interior, girdle view) showing inner foramina (34 in 10 μm).

Figure C15. Rhizosolenia alata.

Rhizosolenia alata Brightwell

The unique morphologic feature separating this species from others in the *Rhizosolenia* genus is the elongated, truncated valve, which does not have a terminal external process. The areolation of the valve wall continues to the extreme distal end, where there is a longitudinal slit (Figure C15a). The distal end is circular in cross section, dentate, and closed by a silicified, recessed plate. It has not yet been determined whether there is anything inside the longitudinal slit but it has been assumed that there might be an internal process (Hasle 1975). The groove into which the valve of the adjacent cell fits is well developed (Fig. C15b). Hasle (1975) reports 50–60 loculi in 10 μm in the bands, 40–50 loculi in 10 μm in the lower part of the valve, and 60 in 10 μm in the finer distal part. In our specimens, loculi in the bands ranged from 40–75 in 10 μm (Figs. C15c and C15d). The round internal foramen is easily observable (Fig. C15c), while the external velum is very difficult to discern. We never observed more than a few bands together (Fig. C15e), presumably a result of the acid cleaning.

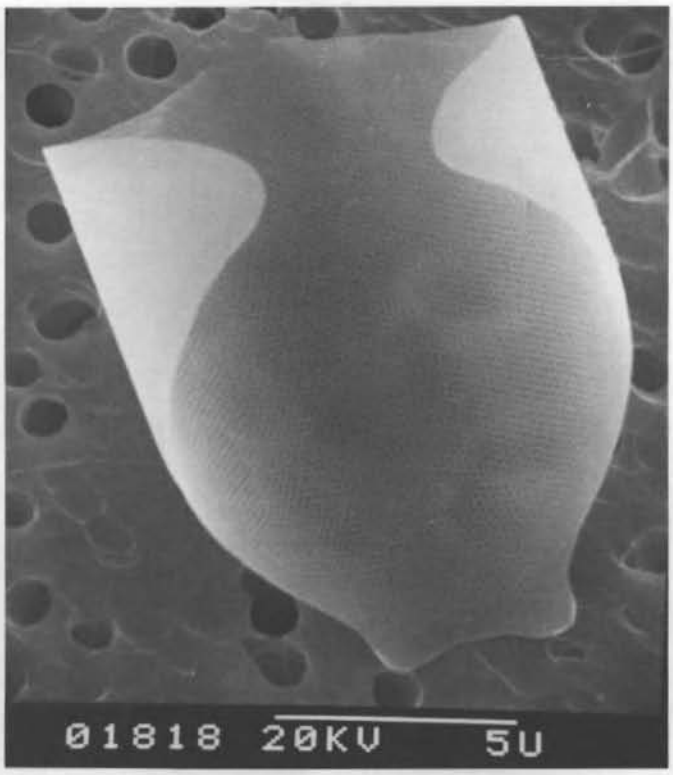

d) Part of band (interior, girdle view) showing inner foramina (64 in 10 μm).

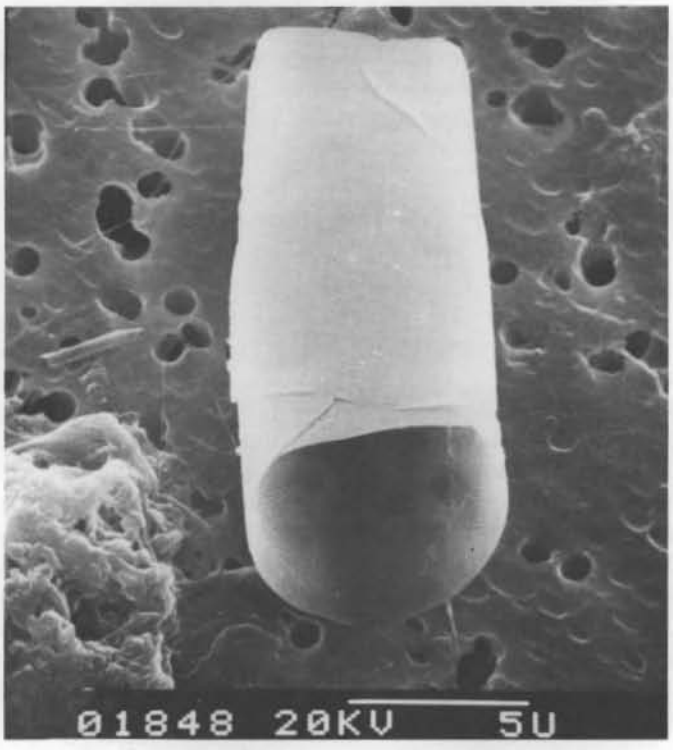

e) Several overlapping bands (oblique, girdle view).

Figure C15 (cont'd).

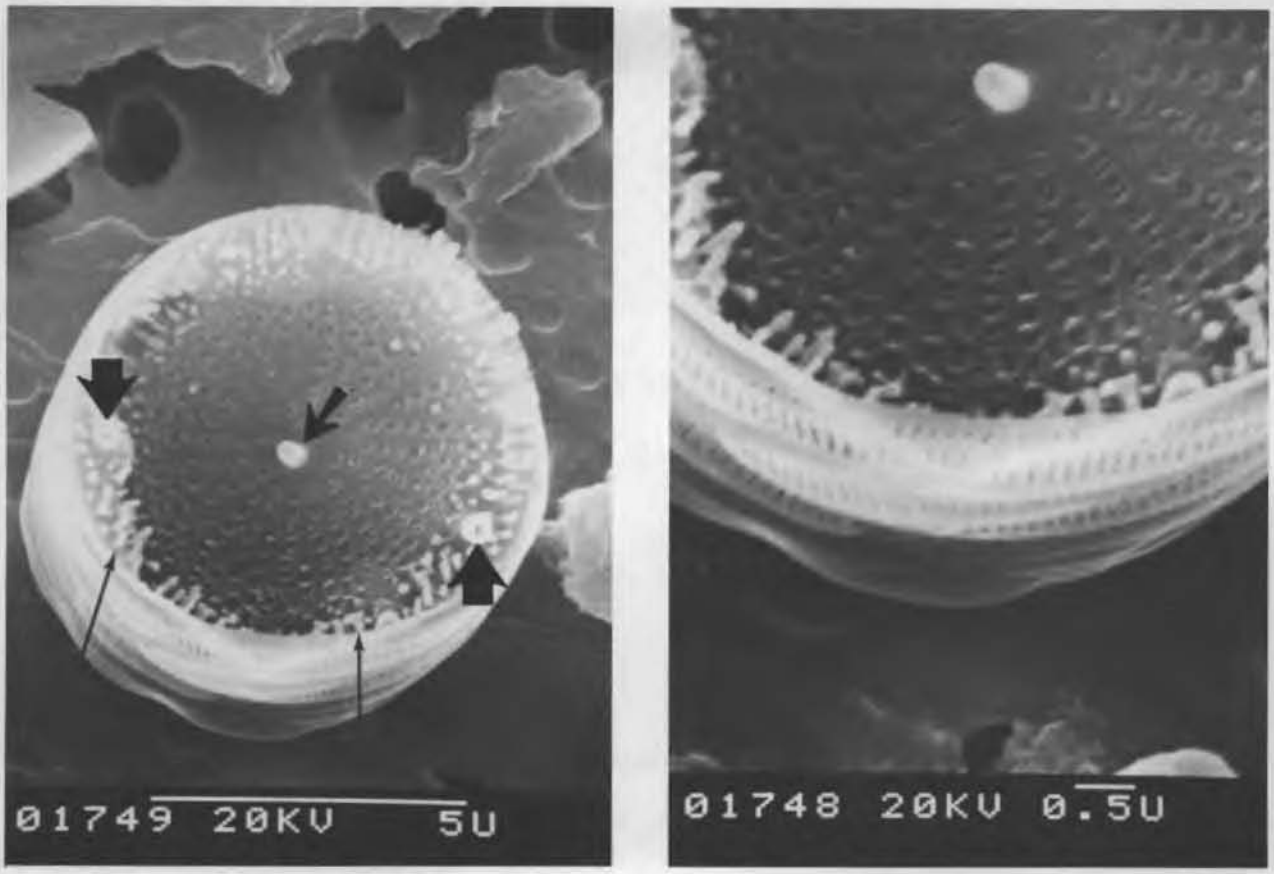

a) Valve and attached girdle bands (oblique view) showing radial pattern of areolation, central (small arrow) and marginal strutted processes (large arrow), and thickened granules (thin arrows).

b) Closeup of same valve showing the thickened granules and girdle bands.

Figure C16. Thalassiosira ambigua.

Thalassiosira ambigua Kozlova

Areolae that appear more or less rectangular and occur in straight radial rows are characteristic of this species (Fig. C16a). The valve diameter reported by Fryxell and Hasle (in press) ranges from 6 to 13 μm with 24 to 32 areolae in 10 μm, with an internal cribrum. Our single specimen was 7 μm in diameter. Between the marginal strutted processes there are 1 to 4 areolae, and between these and the valve margin there is one elongated areolae. The number of marginal strutted processes ranges from 6 to 10 in 10 μm and, while both they and the central strutted process are prominent on the valve face, they do not protrude very far into the valve interior. There is one and sometimes two central marginal strutted processes. Between the marginal processes there is a single labiate process, which is similar to the strutted processes and appears almost flat in the interior with no neck. Externally thickened granules occur between the marginal processes and are more or less well developed depending on the individual (Fig. C16b). The girdle bands are distinctive, the valvocopula having a row of areolate pores adjacent to the valve with a second row of long pores below taking up most of the width of the band. The copula has one row of elongate, areolate pores except at the ligula, where a double row occurs. The remaining four bands are perforate pleurae (Fryxell and Hasle, in press). Unfortunately, while the bands are still attached in our specimen, they are distorted.

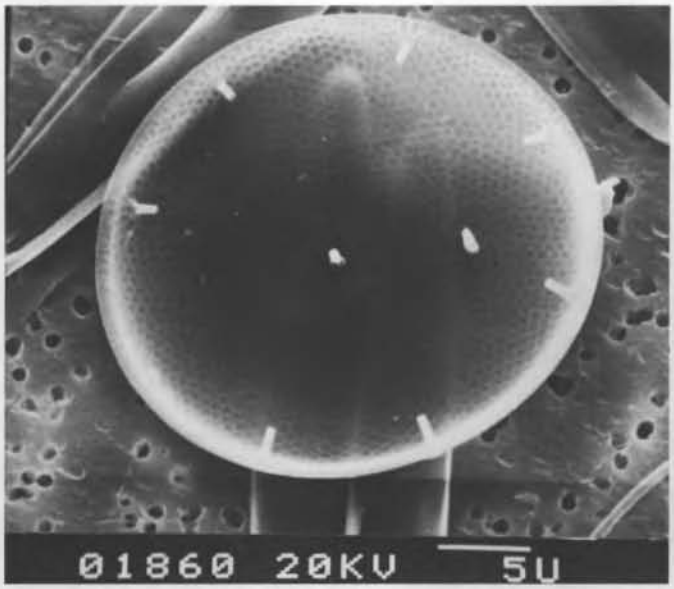

a) Valve (interior) showing pattern of areolation, central and marginal strutted processes (large arrow), and labiate processes (thin arrow) almost directly in line with central process.

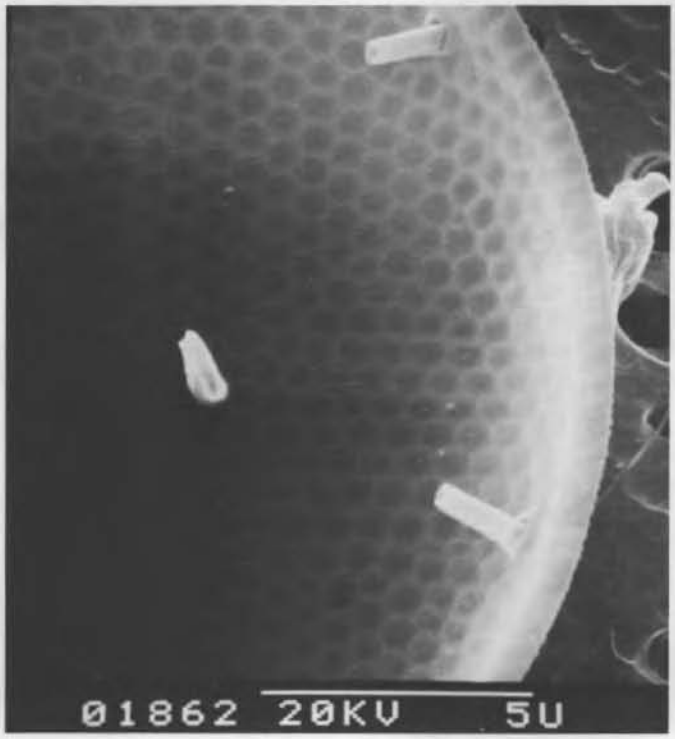

b) Closeup of same valve showing deep penetration of marginal strutted processes and labiate process.

Figure C17. Thalassiosira frenguelli.

Thalassiosira frenguelli Kozolova

This species has areolae in an irregular linear array, 12–20 in 10 μm. There is one central strutted process and a ring of marginal strutted processes (Fig. C17a). The single labiate process, which occurs midway between the margin and the center, is almost directly in line with the central process. Both the labiate and the strutted processes project quite far into the valve interior (Fig. C17b). As far as the girdle bands are concerned there is a perforated valvocopula with a row of large pores adjacent to the valve and several rows of smaller pores towards the copula. The copula also has a row of large pores, while the pleurae are hyaline (Fryxell and Hasle 1979a).

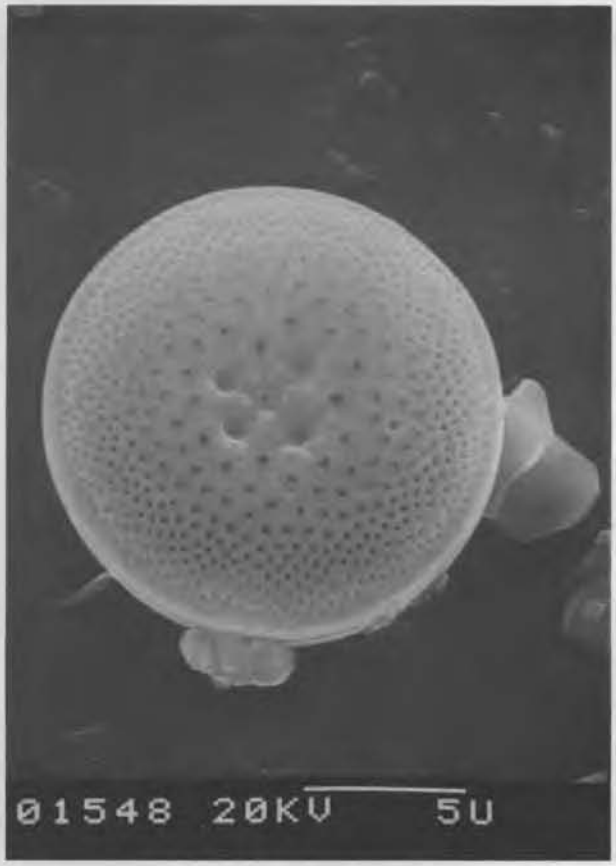

a) Valve view showing that areolae are closer together from the middle to the margin and more widely spaced at the center. Center areolae are not constricted at the surface.

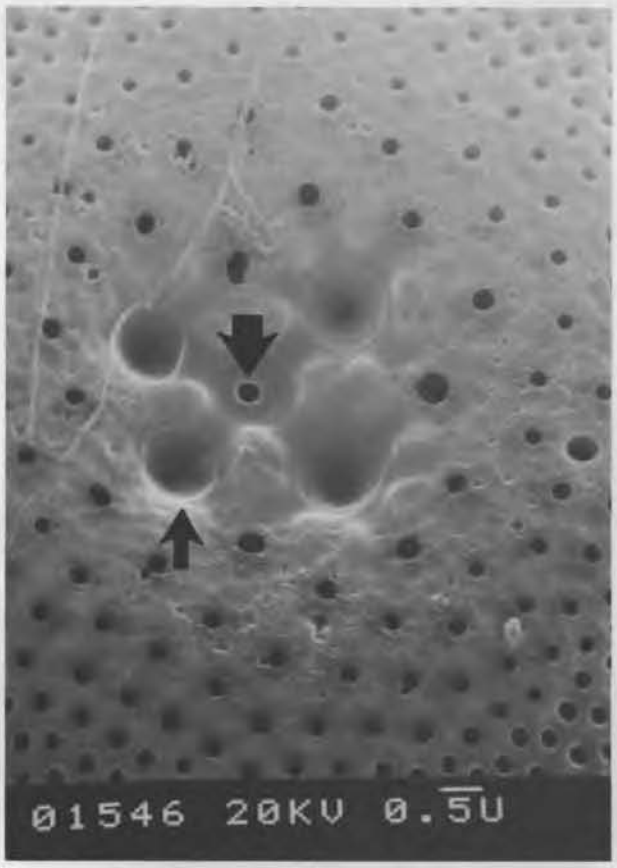

b) Closeup of same valve showing lack of constriction at the surface in the center areolae so that the underlying cribrum is visible (small arrow). Large arrow points to the central strutted process.

Figure C18. Thalassiosira gracilis *var.* gracilis.

Thalassiosira gracilis var. *gracilis* (Karsten) Hustedt

This is a heavily silicified form, 9 to 20 μm in diameter and strongly convex. The areolae are more closely spaced on the mantle and near the margin (25–30 in 10 μm) than they are in the center of the valve (6–12 in 10 μm) (Hasle and Heimdal 1970) as seen in Figure C18a. The foramina are small and constricted except in the center, where there may be no constriction at all of the 4 or 5 central areolae, and the underlying cribrum is visible (Fig. C18b). There are no external extensions of the processes—the central strutted process appears as a hole and the single labiate process as a slit. Internally, the strutted processes extend into the valve and have a modified opercular over the pores in the basal siliceous membrane, as seen in Figure C18c (marginal strutted process) and C18d (central strutted process). There is a direct relationship between the number of marginal strutted processes and the valve diameter. Fryxell and Hasle (1979b) report that their smallest cells had 6 and their largest 28 strutted processes. The range in our samples was from 8 (9-μm diameter) to 15 (15-μm diameter) strutted processes. The single labiate process is small, simple, and located near the margin. The cribra occur as raised rosettes of pores (Fig. C18c).

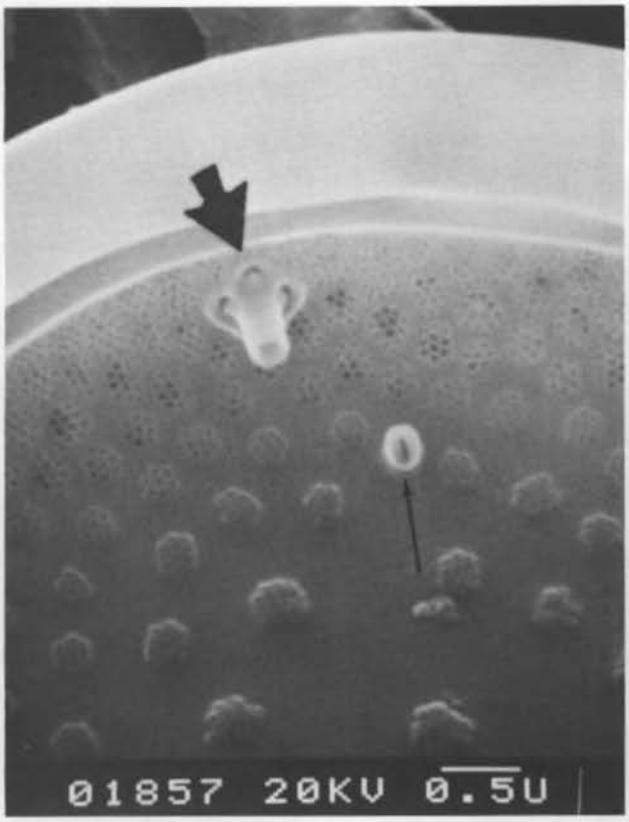

c) Closeup (interior) showing a marginal strutted process with a modified opercular over the pores (large arrow), small labiate process (thin arrow), and the elevated poroid cribrum.

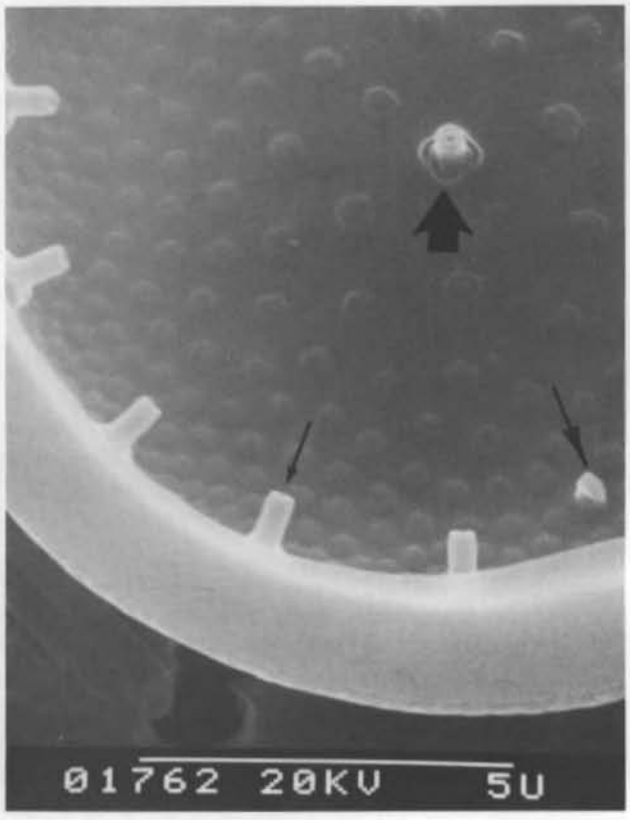

d) Closeup (interior) showing the central strutted process with a modified opercular over the pores (large arrow), the marginal strutted processes (thin arrow), and small labiate process (small arrow).

Figure C18 (cont'd).

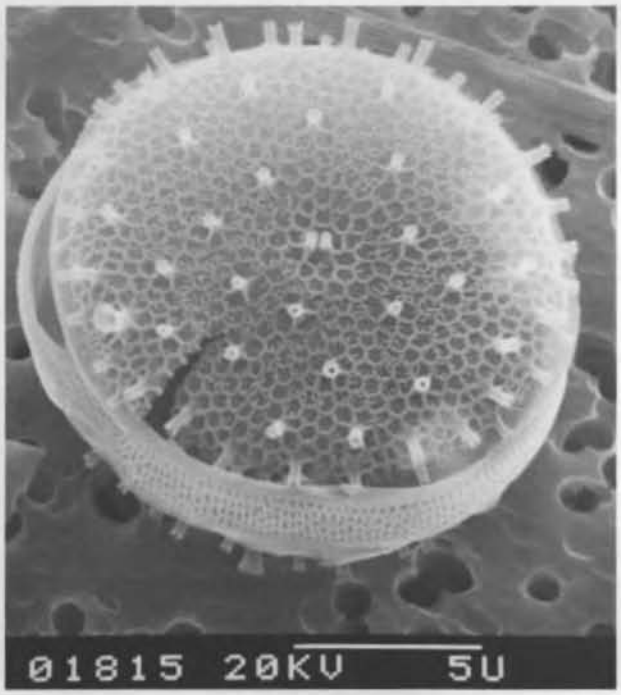

a) Frustule (oblique view) showing scattered strutted processes and pattern of areolation.

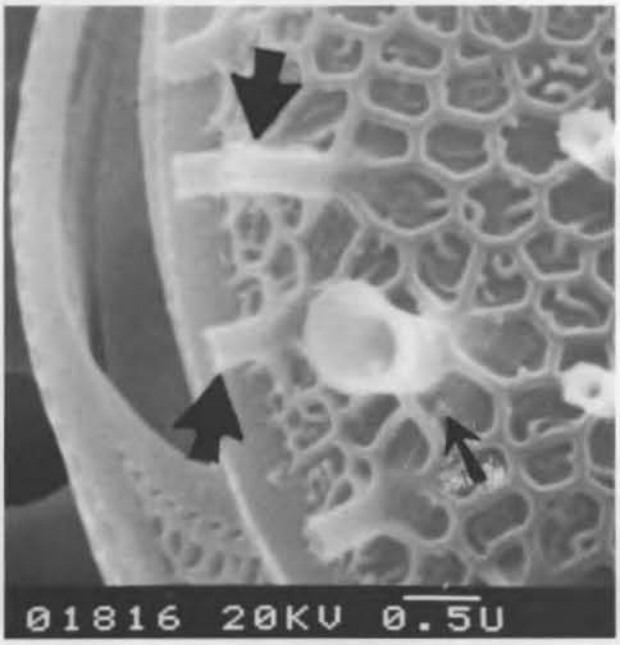

b) Closeup of same valve showing fluted marginal strutted processes (large arrow) and large labiate process (small arrow).

Figure C19. Thalassiosira gravida.

Thalassiosira gravida Cleve

This species has radial rows of areolae, with a tendency to fasciculation. The valve diameter ranges from 13 to 27 μm. There are several central strutted processes, which form a cluster, while additional processes are evenly scattered over the valve face (Fig. C19a). The two rows on the valve mantle have somewhat fluted external tubes (Fig. C19b) while those nearer the center do not (Fig. C19c). Internally, none of the processes is very prominent; the strutted processes have a modified opercula over the pores in the basal siliceous membrane. The labiate, which is both externally and internally larger than the strutted processes, nevertheless has a short neck internally. The unevenly thickened band (Syvertsen 1977) is noted as being characteristic, but only a distorted valvocopula was seen attached to our one frustule (Fig. C19d).

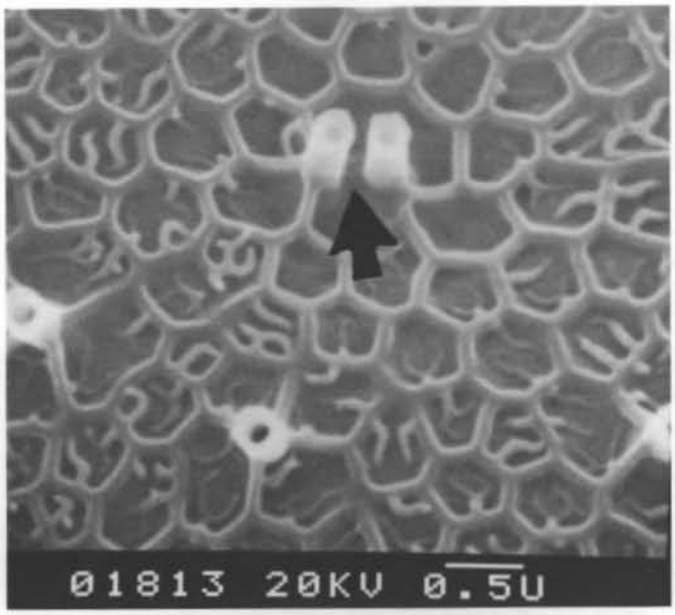

c) Closeup of same valve showing center cluster of two strutted processes (large arrow) and fasciculated pattern of areolae.

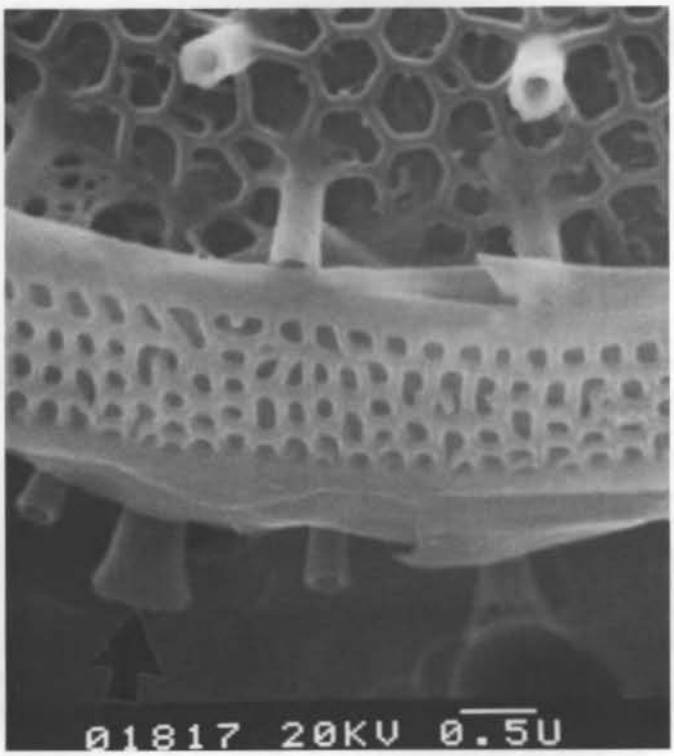

d) Closeup of same valve showing ornate valvocopula and large labiate process of lower valve (large arrow).

Figure C19 (cont'd).

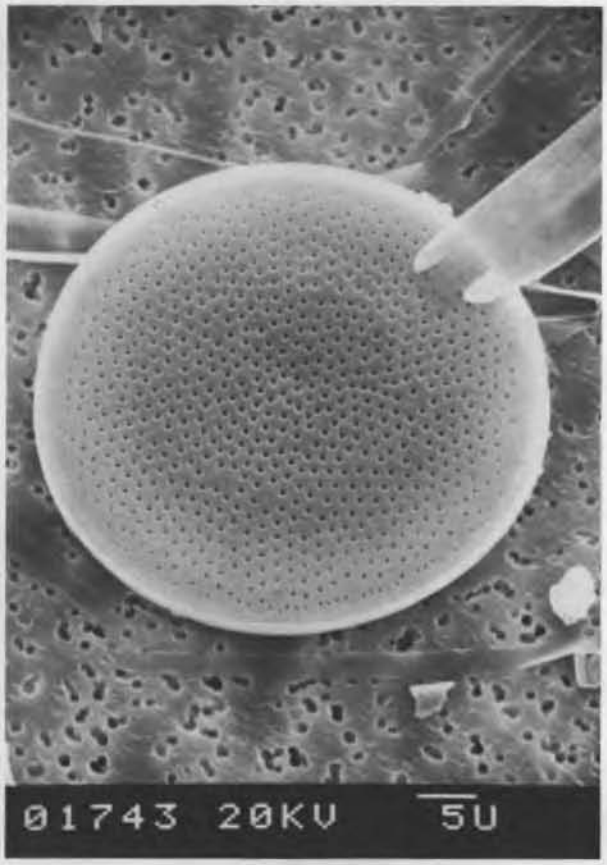

a) Valve view showing radial areolation and scattered strutted processes.

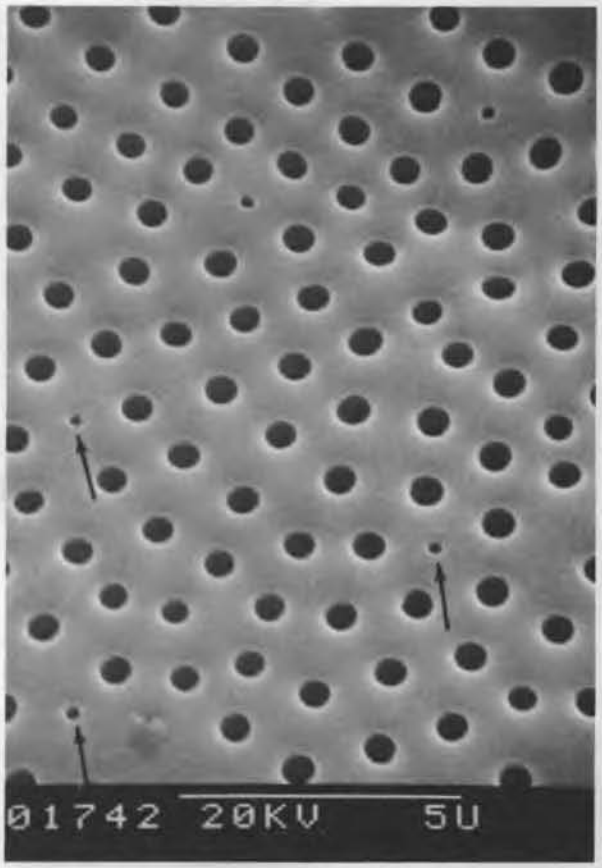

b) Closeup of same valve showing strutted processes taking the place of an areola (thin arrow).

Figure C20. Thalassiosira lentiginosa.

Thalassiosira lentiginosa (Janisch) Fryxell

This species has radial rows of areolae, sometimes irregular and sometimes with fasciculated rows of areolae parallel to a central row. The valve is flat and disk-shaped (Fig. C20a). The diameter reported by Fryxell (1977) is 47–95 μm and by Hendy (1937) is 40–120 μm, while our specimens were 37–70 μm. There are 7–9 areolae in 10 μm. The foramen is external and the strutted processes appear as smaller holes. They are located within the radial rows of areolae and occupy almost the space of an areola, as can be seen in Figure C20b. The marginal strutted processes appear as small holes with a slight indentation (Fig. C20c). The margin is serrated and the number of girdle bands is unknown. The valvocopula has one row of large areolae pores near the valve with several rows of smaller pores below. Externally, the single labiate process appears as a ridge near the margin with a slit on the valve mantle. The cribrum is internal, with the pores in the cribrum oriented in circles (Fig. C20d). Internally, the labiate process also appears as a slit, and the strutted processes are almost flat. The strutted processes are surrounded by four chambers on the margin, but by only two chambers on the valve (Fryxell 1977).

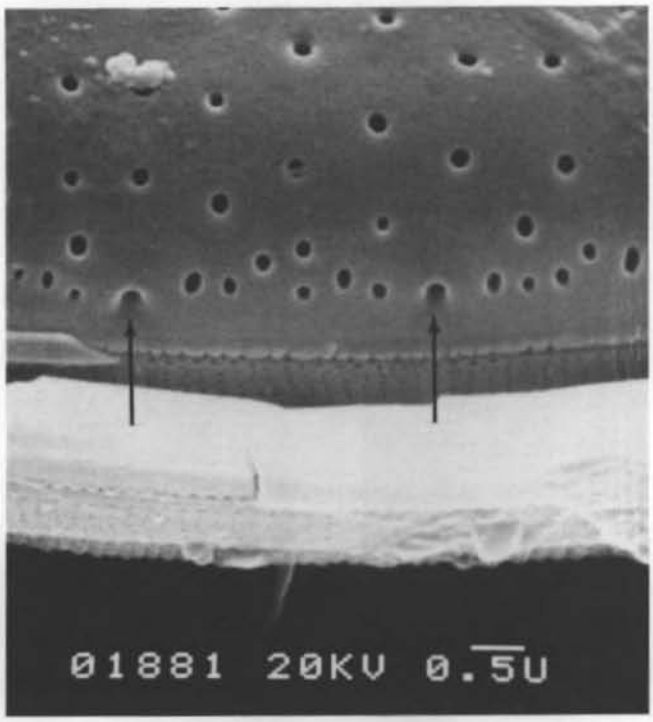

c) Closeup of valve margin showing marginal strutted processes (thin arrows), areolae, and girdle bands.

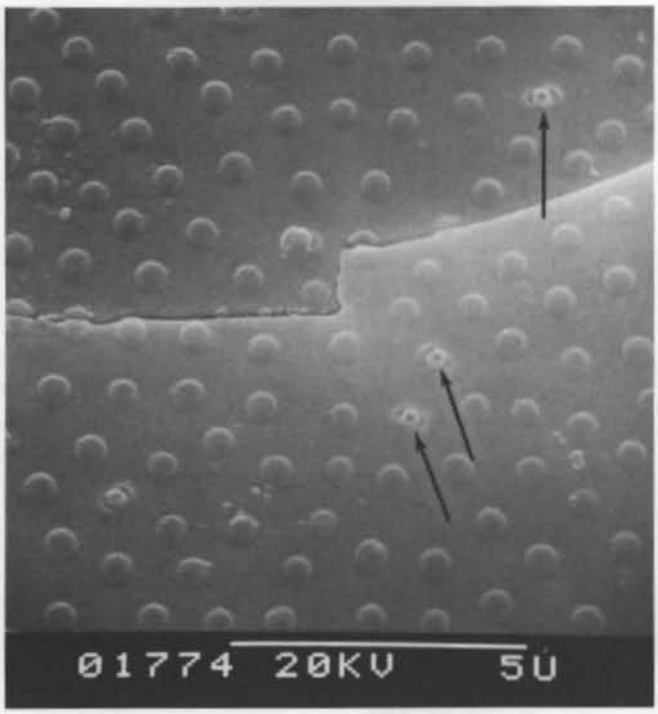

d) Closeup (interior) showing circular cribrum and strutted processes (thin arrows) with minimal internal extension.

Figure C20 (cont'd).

a) Complete frustule (girdle view).

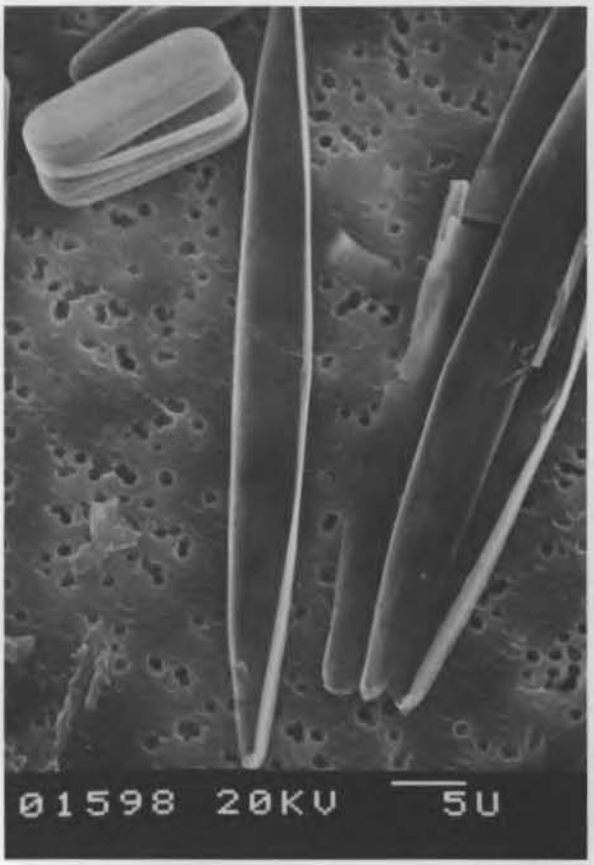

b) Interior and exterior of several valves. Striae are evident in the interior but are covered by a thin silica shell on the outside.

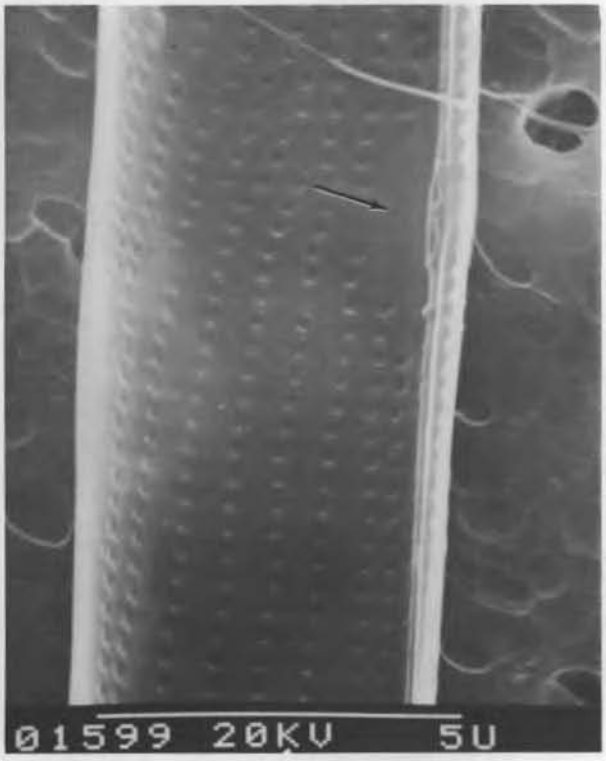

c) Closeup (interior) showing striae (31 in 10 μm), central nodule (arrow), and canal raphe.

In addition to the *Thalassiosira* species described above, we observed two additional species as yet unidentified, and labeled them *Thalassiosira* species 1 and *Thalassiosira* species 2. Since we observed only a single specimen of each, our observations are limited. Until additional specimens are observed, these will not be described.

Tropidoneis glacialis Heiden

Comparing Figures C21a and b, it is evident that the rows of striae (which are composed of fine poroids) visible in the valve interior are covered by a thin silica shell on the exterior. Figure C21c, a closeup of the interior, shows the poroids (31 in 10 μm), central nodule, and canal raphe. Figure C21d is a closeup of the exterior view of the terminal nodule and terminal pore, and Figure C21e, an interior view, shows the infundibulum.

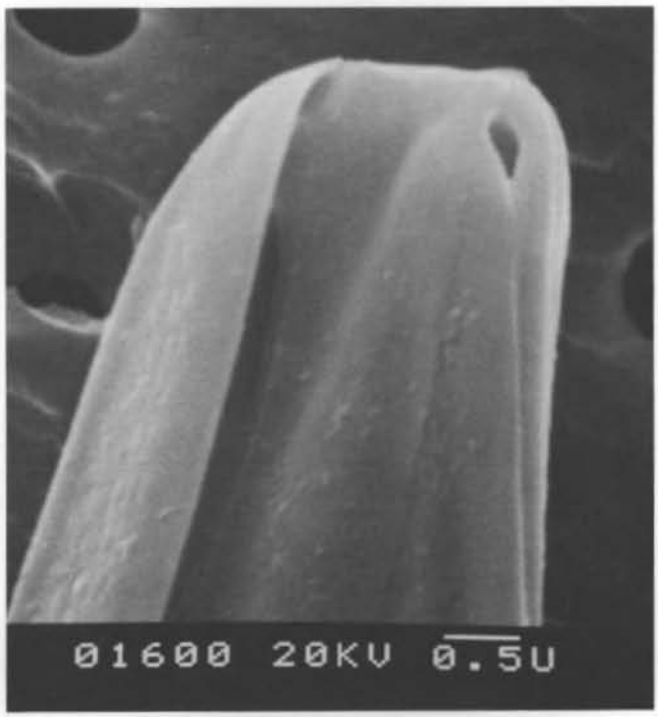

d) Closeup (girdle view) showing terminal nodule, terminal pore, and raphe.

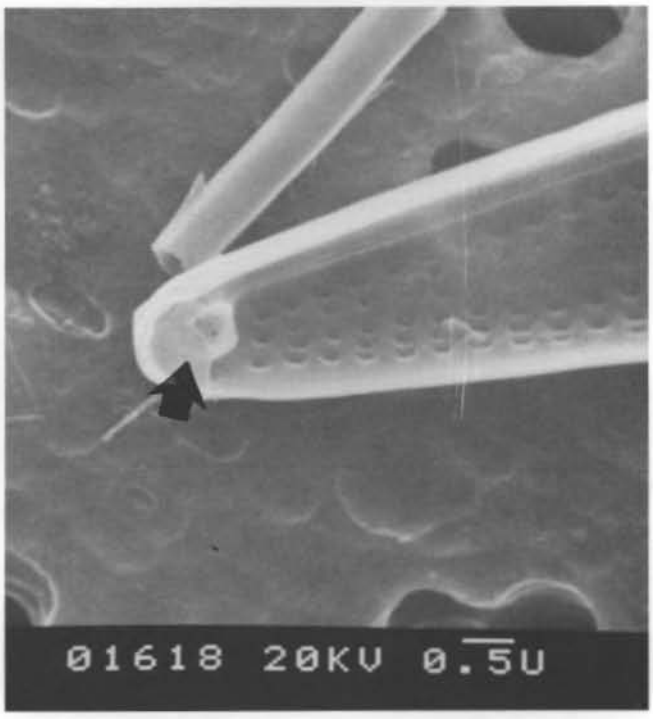

e) Closeup (interior) showing striae and infundibulum (arrow).

Figure C21. Tropidoneis glacialis.